3

Molecular & Nanotechnology

Table of Contents

Interference Lithography

T.B. O'Reilly, H.I. Smith
Sponsorship: Singapore-MIT Alliance

The NanoStructures Laboratory has conducted research on interference lithography (IL) for many years, developing tools and techniques to create periodic structures (such as gratings and grids) over a wide range of spatial periods. The lab currently operates three IL systems. Two of them, the Lloyd's mirror and Mach-Zehnder IL systems use 325 nm light from helium-cadmium lasers. The Lloyd's mirror IL system can be quickly and easily configured to produce gratings with periods as small as 165 nm or as large as many microns. The flexibility and ease of use of this system enables its use by a large number of researchers to produce periodic and quasiperiodic structures for use in a wide range of research programs. The Mach-Zehnder IL system, while less flexible than the Lloyd's mirror, produces higher quality gratings that are suitable for metrological applications. The third system, the Achromatic IL system (AIL) is a grating-based interferometer that writes 100 nm-period gratings using 193 nm light from an ArF excimer laser. In addition, the NSL has close ties to the Space Nanotechnology Lab at MIT, which operates the NanoRuler. The NanoRuler is the most precise IL systems in the world.

We are currently developing a method to characterize photoresist performance by double-exposing a sample on an IL system; the sample is rotated slightly between the two exposures. By analyzing the resulting pattern one can determine how linewidth varies with exposure dose and dose modulation in fewer exposures than are required by previously described methods. The new method is currently being extended to make it possible to model variation of linewidth across the exposure area in systems such as the Lloyd's mirror or Mach-Zehnder IL systems.
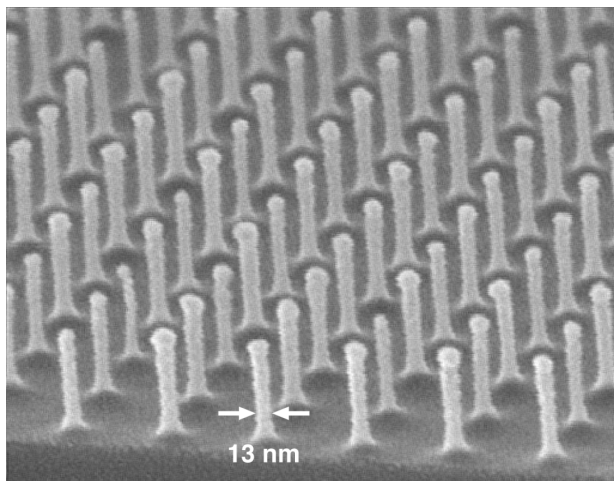
▲ Figure 1: Scanning electron micrograph of a 100 nm-period grid produced with the AIL system. PMMA was exposed on top of an antireflection coating and the pattern was transferred into Si by reactive ion etching.

13 nm
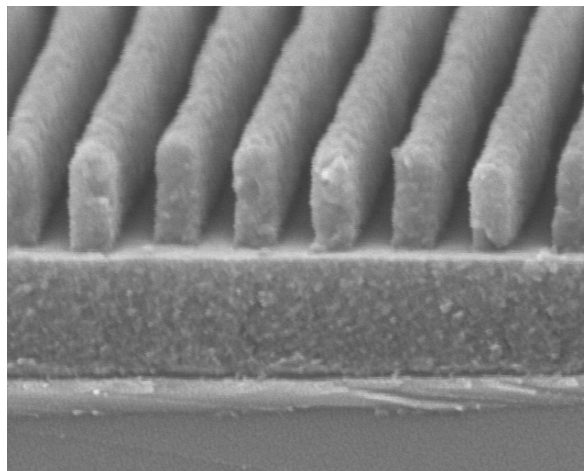
▲ Figure 2: Micrograph of 165 nm period grating produced with the Lloyd's mirror in photoresist above an antireflection coating. The Lloyd's mirror system can be used to produce patterns with spatial periods ranging from 165 nm up to several microns.

Reference

[1] T.B. O'Reilly and H.I. Smith, "Photoresist characterization using double exposures with interference lithography," *Journal of Vacuum Science and Technology B*, vol. 26, no. 1, pp. 128-131, 2008.

Scanning Beam Interference Lithography

M. Ahn, C.-H. Chang, R. Heilmann, Y. Zhao, M.L. Schattenburg
Sponsorship: NASA

Traditional methods of fabricating gratings, such as diamond-tip ruling, electron and laser-beam scanning, or holography, are generally very slow and expensive and result in gratings with poor control of phase and period. More complex periodic patterns, such as gratings with chirped or curved lines, or 2D and 3D photonic patterns, are even more difficult to pattern. This research program seeks to develop advanced interference lithography tools and techniques to enable the rapid patterning of general periodic patterns with much lower cost and higher fidelity than current technology.

Interference lithography (IL) is a maskless lithography technique based on the interference of coherent beams. Interfering beams from an ultra-violet laser generates interference fringes that are captured in a photo-sensitive polymer resist. Much of the technology used in modern IL practice is borrowed from technology used to fabricate computer chips. Traditional IL methods result in gratings with large phase and period errors. We are developing new technology based on interference of phase-locked scanning beams, called scanning beam interference lithography (SBIL). The SBIL technique

has been realized in a tool called the MIT Nanoruler, which recently won a R&D 100 Award (Figure 1). Large gratings can be patterned in a matter of minutes with a grating phase precision of only a few nanometers and a period error in the ppb range.

Current research efforts seek to generalize the SBIL concept to pattern more complex periodic patterns, such as variable period (chirped) gratings, 2D metrology grids, and photonic patterns [1]. Important applications of large, high fidelity gratings are for high-resolution x-ray spectroscopes on NASA x-ray astronomy missions, high-energy laser pulse compression optics, and length metrology standards. We have recently developed a new grating patterning technique called aligned multiple overlay SBIL, which uses multiple (up to four) precisely overlaid IL images to divide the fundamental grating pattern down to very short periods, in this case 50-nm-pitch, over large areas (Figure 2). This type of pattern has many applications including nanomagnetics, semiconductor, and nanobiologic manufacturing.
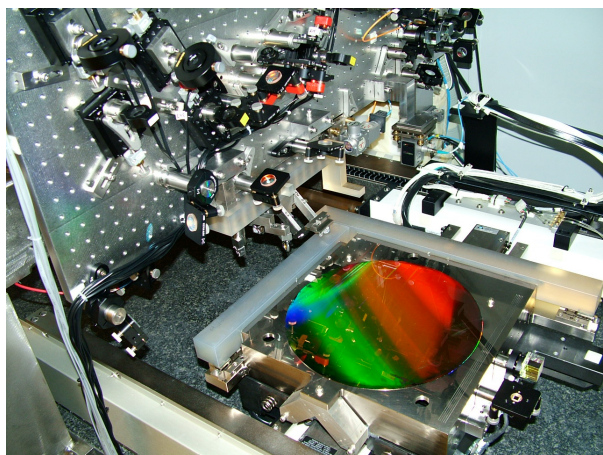
▲ Figure 1: Photograph of the Nanoruler lithography and metrology system built by MIT students. This unique tool is the most precise grating patterning and metrology system in the world.
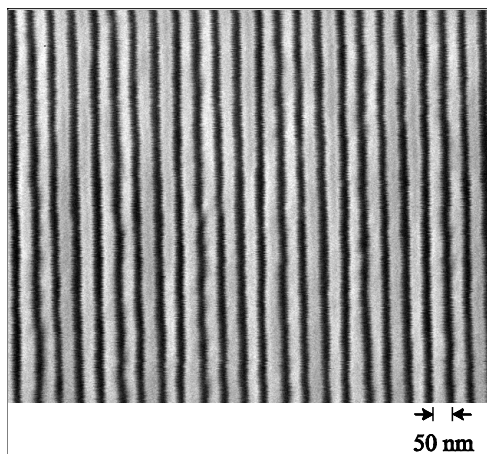
▲ Figure 2: A 50-nm-pitch (25-nm-line/space) grating pattern fabricated by 4X overlaid interference lithography.

References

[1] G.S. Pati, R.K. Heilmann, P.T. Konkola, C. Joo, C.G. Chen, E. Murphy, and M.L. Schattenburg, "A generalized scanning beam interference lithography system for patterning gratings with variable period progressions," *Journal of Vacuum Science Technology B*, vol. 20, pp. 2617-2621, 2002.

[2] P. Konkola, C. Chen, R.K. Heilmann, C. Joo, J. Montoya, C.-H. Chang, and M.L. Schattenburg, "Nanometer-level repeatable metrology using the Nanoruler," *Journal of Vacuum Science Technology B*, vol. 21, pp. 3097-3101, 2003.

[3] J. Montoya, C.-H. Chang, R.K. Heilmann, and M.L. Schattenburg, "Doppler writing and linewidth control for scanning beam interference lithography," *Journal of Vacuum Science Technology B*, vol. 23, pp. 2640-2645 (2005).

[4] Y. Zhao, C.-H. Chang, R.K. Heilmann, and M.L. Schattenburg, "Phase control in multiexposure spatial frequency multiplication," *Journal of Vacuum Science Technology B*, vol. 25, pp. 2439-2443, 2007.

[5] C.-H. Chang, R.K. Heilmann, M.L. Schattenburg, and P. Glenn, "Design of a double-pass shear mode acousto-optical modulator," *Review of Scientific Instruments*, vol. 79, pp. 033104:1-5, 2008.

Immersion-Achromatic-Interference Lithography for Sub-100 nm-Period Structures

T.B. O'Reilly, H.I. Smith
Sponsorship: Singapore-MIT Alliance, Lincoln Laboratory

Interference lithography (IL) is a means of using the coherent interference of light to produce periodic patterns. The spatial period, *P*, produced is dependent on the interference angle θ, wavelength of light, λ, and the refractive index of the incident medium, *n*, and is given by: $P = \lambda / 2n\sin(\theta)$. Reducing the period of the pattern is most commonly accomplished by reducing λ or increasing θ. As the interference angle cannot exceed 90°, and the selection of suitable short-wavelength sources is limited, reduction of *P* below λ/2 requires the use of an immersion fluid to reduce the effective wavelength of the light.

We are presently developing an immersion achromatic interference lithography system to extend our capability to produce fine-period patterns. The system being developed is similar to the lab's existing achromatic IL system, which produces 100 nm-period gratings, in that the new immersion system will use diffraction gratings to split and recombine 193 nm light from an ArF excimer laser. The addition of an immersion fluid, initially water, will allow the system to write patterns with periods of 70 nm. Use of higher index fluids will make it possible to write even finer patterns. Development of fabrication processes for the gratings is currently underway.

Gratings and grids produced with this tool will likely find applications similar to those produced by the existing AIL system, which includes templates for self assembly and gratings for atom-interferometry. The system could also be used to test materials including photoresists and immersion fluids at periods smaller than are possible with other lithography systems.
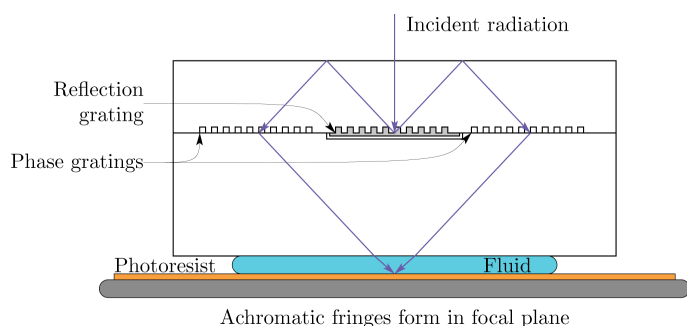
▲　Figure 1: Schematic diagram of immersion achromatic IL system under development. Light from an excimer laser enters vertically at the top of the interferometer and is diffracted by a reflection grating. The light reflects off the top of the interferometer where a pair of transmission gratings diffract the light back toward the focal plane where it exposes a photosensitive substrate.
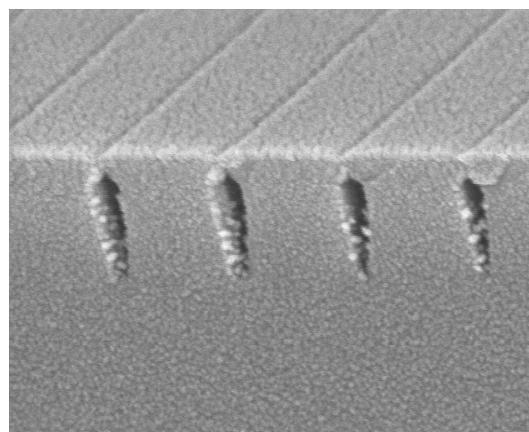
▲　Figure 2: Transmission grating fabricated in glass with a period of 266 nm. The geometry of the grating must be carefully controlled to get reasonable diffraction efficiency into the desired orders, which presents a fabrication challenge.

Spatial-phase-locked Electron-beam Lithography

E.E. Moon, H.I. Smith, J.T. Hastings (U. Kentucky)
Sponsorship: NSF

Our research in spatial-phase-locked electron-beam lithography (SPLEBL) is conducted in collaboration with the University of Kentucky. It is aimed at reducing pattern-placement errors in electron-beam-lithography systems to the sub-1 nm level. Such high precision is essential for certain applications in photonics and nanoscale science and engineering. SPLEBL is currently the only approach capable of achieving such pattern-placement accuracy. As shown in Figure 1, SPLEBL uses a periodic signal, derived from the interaction of the scanning e-beam with a fiducial grid placed directly on the substrate, to continuously track the position of the beam while patterns are being written. Any deviation of the beam from its intended location on the substrate is sensed, and corrections are fed back to the beam-control electronics to cancel beam-position errors. In this manner, the locations of patterns are directly registered to the fiducial grid on the substrate.

The research effort at MIT is now focused on developing the materials and processes for producing the fiducial grid, with the objectives of: maximizing the signal-to-noise of the secondary-electron signal derived from the grid; minimizing electron scattering from the grid, which would be deleterious to precision lithography; maximizing the area and absolute accuracy of the grid; and minimizing the cost and inconvenience of producing the grid on substrates of interest. We have determined that signal levels are maximized when the grid is formed from nanoparticles. Substrates have been patterned with in-situ Faraday cups to make accurate measurements of signal-to-noise for a wide variety of nanoparticle types. To minimize electron scattering, the nanoparticles must be composed of low-atomic-number materials. Fullerenes may be the optimal nanoparticle, but achieving uniform thickness of layers and attaching the fullerenes along the grid lines represents a challenge of attachment chemistry. Scanning-beam interference lithography will be used to produce master grids. A special form of imprint lithography that maintains long-range spatial-phase coherence and conformal contact will be used to transfer attachment-chemistry grid patterns onto substrates of interest.

The research effort at the University of Kentucky is focused on processing of the signal from the grid. Specifically, new approaches are being developed that enable spatial-phase locking while e-beam writing in a vector-scan mode. Previous approaches utilized only the raster-scan mode.
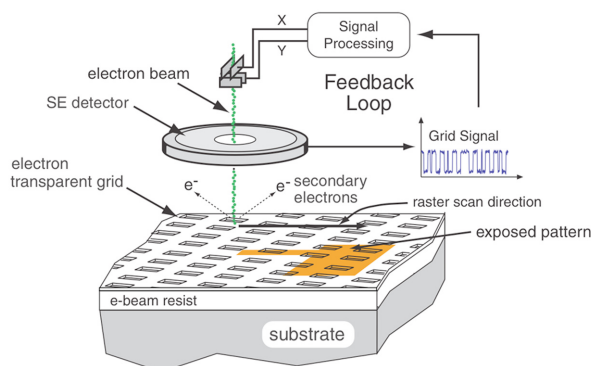
▲ Figure 1: Schematic of the global-fiducial-grid mode of spatial-phase-locked electron-beam lithography. The periodic signal detected from the fiducial grid, which includes both X and Y components, is used to measure placement error, and a correction signal is fed back to the beam deflection system.

References
[1] J.T. Hastings, F. Zhang, and H.I. Smith, "Nanometer-level stitching in raster-scanning e-beam lithography using spatial-phase locking," *Journal of Vacuum Science and Technology B*, vol. 21, no. 6, pp. 2650-2656, Nov/Dec 2003.
[2] F. Zhang, H.I. Smith and J.F. Dai, "Fabrication of high-secondary-electron-yield grids for spatial-phase-locked electron-beam lithography," *Journal of Vacuum Science and Technology B*, vol. 23, no. 6, pp. 3061-3064, Nov/Dec 2005.

Optimum Exposure Parameters for High-resolution Scanning Electron-beam Lithography

B. Cord, J. Yang, K.K. Berggren
Sponsorship: NRI, King Abdulaziz City for Science and Technology and Alfaisal University, MIT

The resolution of a scanning electron-beam lithography (SEBL) exposure process is primarily limited by two processes: (1) the range of forward scattering of the incident beam and (2) the range of secondary electrons produced by interactions between the primary beam and the resist [1, 2]. The forward-scattering behavior has been well-characterized, and its extent is known to be proportional to the resist thickness and inversely proportional to the primary beam energy [3]. The behavior of the secondary electrons is less well-documented, but their approximate range is thought to be independent of resist thickness and either independent of [2] or weakly proportional to [4] the primary beam energy.

The dependencies of these two limiting factors suggest that, for a given resist thickness, there exists a "crossover" energy at which the process is balanced between the forward-scattering- and secondary-electron-limited regimes and any further increase in the beam energy results in no increased resolution. While it has been hypothesized that secondary-electron range is the main resolution limiter in most thin-resist applications [1], the energies at which forward scattering becomes irrelevant have never been determined.

Using Monte Carlo simulations [5], we have calculated both the forward-scattering length and average secondary electron range over a range of beam energies and resist thicknesses (see Figure 1). The results suggest that, for resists thinner than 100 nm, the crossover beam energy occurs at approximately 30-40 keV, suggesting in turn that thin-resist lithographic resolution on relatively low-cost 30 keV SEBL tools may be equal or superior to that attainable on high-end, high-beam-energy systems. This hypothesis is partially supported by the micrographs in Figure 2, which demonstrate sub-10-nm lithographic resolution in 35-nm-thick films of HSQ [6] using MIT's 30 keV Raith-150 SEBL tool.
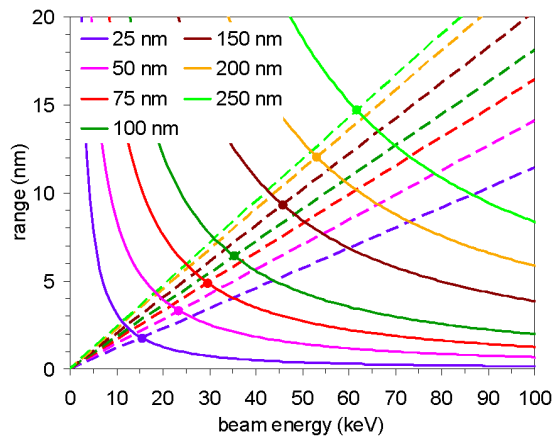
▲ Figure 1: Curve fits of Monte Carlo results for the forward-scattering length α (solid lines) and the secondary electron range λ (dashed lines) as a function of beam energy for various resist thicknesses. The crossover points, indicating the beam energy at which the resolution is maximized, are marked with dots.
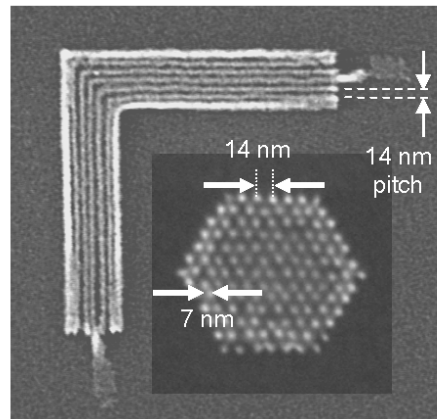
▲ Figure 2: A 7-nm-wide nested "L" and dot (inset) features on a 14-nm-pitch, exposed in 35 nm of HSQ at 30 keV using the Raith-150 SEBL tool at MIT.

References

[1] A.N. Broers, "Resolution limits for electron-beam lithography," *IBM Journal of Research and Development*, vol. 32, no. 4, pp. 502-513, 1988.
[2] D.C. Joy, "The spatial resolution limit of electron lithography," *Microelectronic Engineering*, vol. 1, no. 2, pp. 103-119, Oct. 1983.
[3] R.J. Hawryluk, "Exposure and development models used in electron beam lithography," *Journal of Vacuum Science and Technology*, vol. 19, no. 1, pp. 1-17, May 1981.
[4] M. Bolorizadeh and D.C. Joy, "Effects of fast secondary electrons to low-voltage electron beam lithography," *Journal of Micro/Nanolithography, MEMS and MOEMS*, vol. 6, no. 2, pp. 023004:1-7, Apr.-June 2007.
[5] P. Hovington, D. Drouin, and R. Gauvin, "CASINO: A new Monte Carlo code in C language for electron beam interaction – Part I: Description of the program," *Scanning*, vol. 19, no. 1, pp. 1-14, 1997.
[6] J.K.W. Yang and K.K. Berggren, "Using high-contrast salty development of hydrogen silsesquioxane for sub-10-nm half-pitch lithography," *Journal of Vacuum Science and Technology B*, vol. 25, no. 6, pp. 2025-2029, Nov. 2007.

High-resolution Nanoimprint Lithography

D. Morecroft, J.K.W. Yang, K.K. Berggren
Sponsorship: Quantum Nanostructures and Nanofabrication Group, RLE, MIT

Nanoimprint lithography (NIL) is quickly maturing as a next-generation patterning technique that offers the combined advantages of high resolution, low cost and high throughput [1]. Unlike conventional optical lithography techniques, NIL physically imprints a 3D-structured mold into resist. The mold imprints the inverse pattern, which can then be transferred into the substrate by reactive-ion etching. While nanoimprint lithography is attractive as a low-cost high-throughput technique, the fabrication of its imprint mold still depends on other lithography methods. A key issue to resolve is the ultimate pitch resolution of the patterns since this factor determines the upper limit of the density. In this work we combine the high-resolution capabilities of electron-beam lithography with the high throughput of nanoimprint to obtain densely packed nanostructures over a large surface area.

Previously results have shown that negative tone resist can be used in combination with a salty developer technique to enhance contrast [2]. With this technique, hydrogen silsesquioxane (HSQ) resist was spun onto silicon substrate with a thickness of 20 nm, and electron-beam lithography was carried out using a Raith 150 EBL tool with a 30-kV acceleration voltage. The patterns were developed in an aqueous solution of 1% NaOH, 4% NaCl, and pattern transfer into the silicon was carried out using reactive-ion etching in a Plasma Therm 770 with a HBr plasma. Figure 1 shows a tilted scanning electron micrograph of 25-nm-pitch square-packed dots after reactive ion etching with a depth profile of 35 nm. The results show good profile transfer between the HSQ and silicon. The patterned silicon substrate was then used as a mold for nanoimprint lithography, and Figure 2 shows a 36-nm-pitch hexagonal dot array successfully transferred into the nanoimprint resist.

There are many potential applications for this patterning process, for example nanopatterned electrodes for fuel cells and batteries, where the increased surface area may enhance the catalytic activity.
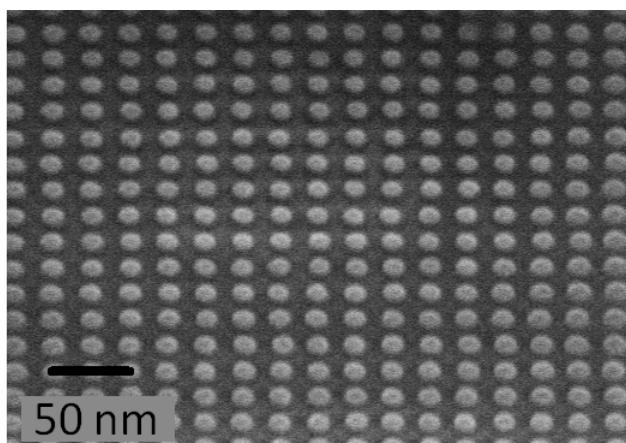
▲   Figure 1: Tilted scanning micrograph of 25-nm-pitch pillars after reactive-ion etching with a hydrogen bromide plasma into the silicon substrate.
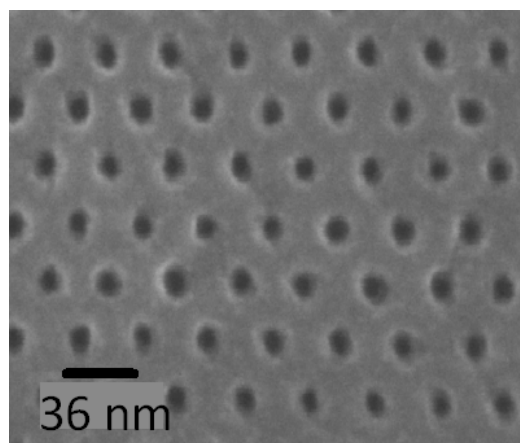
▲   Figure 2: Scanning electron micrograph of 36-nm-pitch dots imprinted into nanoimprint resist with 4-nm Ti for imaging.

References
[1]   S.Y. Chou, P.R. Krauss, and P.J. Renstrom, "Imprint lithography with 25-nm resolution," *Science*, vol. 272, pp. 85–87, Apr. 1996.
[2]   J.K.W. Yang and K.K. Berggren, "Using high-contrast salty development of hydrogen silsesquioxane for sub-10-nm half-pitch lithography," *Journal of Vacuum Science and Technology B*, vol. 25, no. 6, pp. 2025-2029, Nov. 2007.
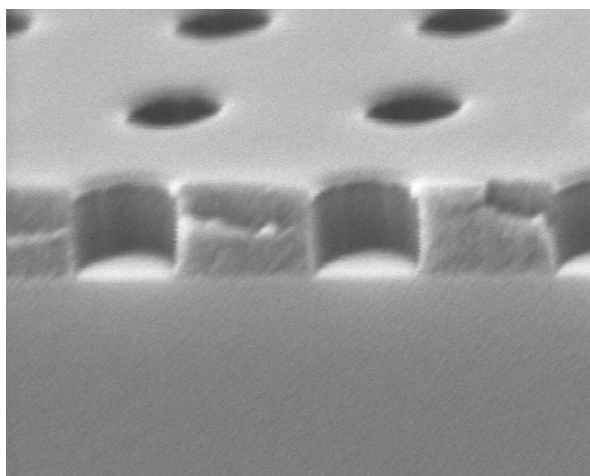
Fabrication of Inverted-Pyramid Arrays in Si for Templated Self Assembly

T. Savas, T.B. O'Reilly, H.I. Smith
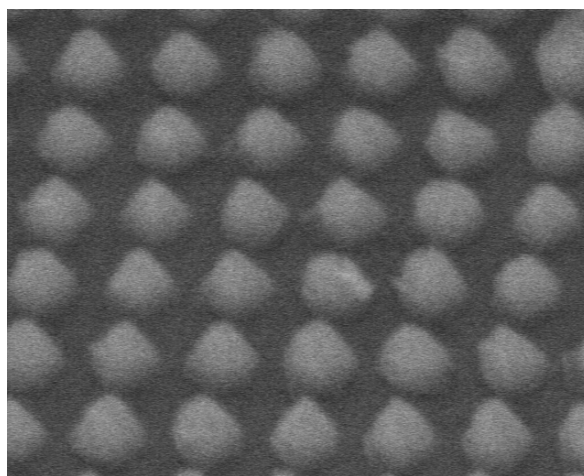Sponsorship: Singapore-MIT Alliance

Recently, in support of the Singapore-MIT Alliance, the lab's interference-lithography (IL) was used to fabricate two types of patterned substrates for use in research on templated self-assembly.

The first set of substrates was fabricated to support research on the interaction of materials with inverted pyramids etched into silicon. The fabrication begins by depositing a thin layer of SiO_2 on a (100) silicon wafer. A tri-layer resist stack is deposited on the substrate, and the resist is patterned by interference lithography, in this case using the Lloyd's mirror IL system. Following development of the exposed resist, the pattern is transferred to the substrate using reactive-ion-etching, forming a grid of holes in the SiO_2 layer. The Si substrate is then etched in KOH, which preferentially etches into the <100> direction much faster than into the <111> direction, resulting in the formation of inverted-pyramids where each of the holes in the SiO_2 was located. Various materials can then be deposited or grown on the patterned substrate to determine how the surface patterning affects the material response.

A second set of substrates was fabricated for use in experiments on nanoporous aluminum oxide, which is formed by oxidizing aluminum under certain conditions. The process leads to the formation of many nanoscale pores perpendicular to the surface which generally have some characteristic spacing, but no long-range order. To provide long-range order in the pattern of pores, a silicon-rich silicon-nitride membrane was patterned using interference lithography. Reactive-ion-etching and liftoff were used to form an array of chromium cones on the membrane. By pressing the membrane into an aluminum surface with air-pressure on the backside the cones could be used to form small dents in the surface to determine if that would affect the location of the pores that would form when the aluminum was later oxidized.

▲ Figure 1: Micrograph of a stage in the preparation of a substrate containing an array of inverted-pyarmids, for use in research on templated self-assembly. A pattern consisting of a grid of holes, with a spatial period of 200 nm, was written using interference lithography and has been transferred to the substrate by reactive ion etching. Due to differences in the etch rates of different crystal planes, etching this substrate in KOH will form inverted pyramids in the silicon substrate.

▲ Figure 2: Micrograph showing a 200 nm-period grid of chrome cones on a silicon-nitride membrane. The pattern was created by interference lithography, and the cones were formed by a combination of etching and liftoff. These cones were formed for use in indenting an aluminum surface to control the positions of the pores in nanoporous aluminum oxide.

Fabrication of Suspended Discs in Si$_3$N$_4$ Membranes for Observation of the Poisson Spot with Deuterium

A.A. Patel, T. Reisinger (Univ. Graz, Austria), B. Holst (Univ. Graz, Austria), H.I. Smith
Sponsorship: Univ. Graz, Austria, internal funds

The observation of a bright central spot in the shadow of an opaque circular object, the so-called Poisson Spot, was an historically important experiment establishing the wave nature of light. The same interference phenomenon should occur with material particles. To conduct an experiment to observe the Poisson Spot with monochromatic deuterium molecules, we fabricated free-standing discs of silicon nitride, shown in Figure 1.

The discs had a diameter of 100 μm and a thickness of 500 nm, centered within a 400 μm-diameter window and supported by four 3μm-wide support bars. The key parameters for the disc include thickness, ellipticity and edge roughness. Scanning-electron-beam lithography was used to pattern the area of the disc and the support bars on a Si$_3$N$_4$ membrane. PMMA was used as the electron-beam resist, and the pattern was transferred to a chromium hardmask via a wet etch. The area of the disc and in between the support bars was etched away using reactive ion etching. Figure 1 shows a final device in Si$_3$N$_4$. Figure 2 shows the observation of the Poisson Spot through experiments run by our colleagues at the University of Graz in Austria.
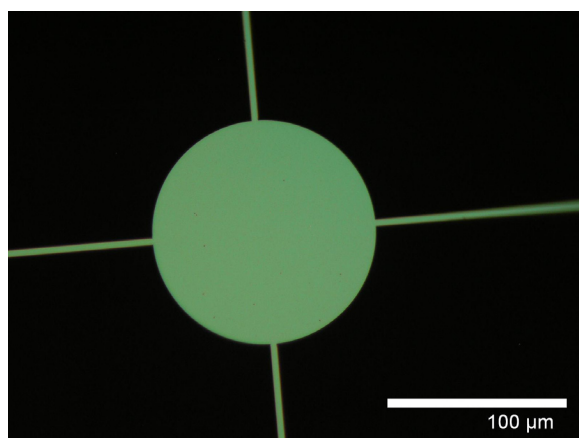
▲ Figure 1: Optical micrograph of the most recently fabricated free-standing disc. (There is no material in the dark regions.) The disc obstruction is 100 μm in diameter and about 500 nm thick. SEM metrology showed that edge roughness was under 50 nm.
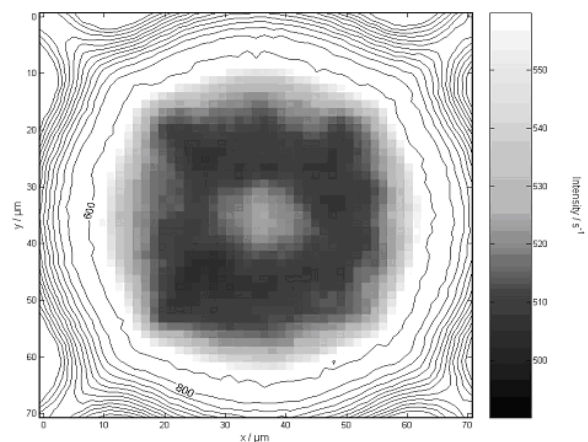
▲ Figure 2: Deuterium Poisson Spot. Shown is the first Poisson Spot realized with molecules. The central part of the shadow is amplified as a grey image plot. The image is the sum of 24 images recorded consecutively at a sampling distance of 321 mm.

Reference

[1] T. Reisinger, G. Bracco, S. Rehbein, S. Schmahl, W. E. Ernst, B. Holst, "Direct Images of the Virtual Source in a Supersonic Expansion," *Journal of Physical Chemistry* vol. A76, pp. 12620-12628, 2007.

Correction of Intrafield Distortion in Scanning-Electron-Beam Lithography and Confirmation via Optical Ring-Resonator Filters

J. Sun, C.W. Holzwarth, J.T. Hastings (U. Kentucky), H.I. Smith
Sponsorship: DARPA

In scanning-electron-beam lithography (SEBL), distortion in the electron-beam deflection field (i.e., intrafield distortion) leads to systematic pattern-placement errors. These are particularly detrimental to photonic devices, which depend on coherent interference. Intrafield distortion arises from imperfections in the electron optics, and errors in the digital-to-analog conversion and field-calibration electronics. The intrafield distortion of our Raith 150 SEBL system was measured by comparing a written grid to a precision reference grid, generated by interference lithography. Figure 1 is a map of the Raith's intrafield distortion for a 100μm field.

Optical microring-resonator filters in high-index-contrast materials, such as Si or Si_3N_4, require 1-nm-level pattern-placement precision. In fabricating such devices with SEBL, intrafield distortion is manifested in the deviation of resonant frequency from design val-

ues. Figure 2 shows a typical transmission spectrum of a 2nd-order microring-resonator filter in which the resonant frequencies of the two rings are shifted by 20.5 GHz. Based on the measured distortion map, we calculated the expected resonant-frequency mismatch as a function of position and orientation in the SEBL exposure field. Figure 3 shows the results, with the boxes enclosing experimental resonant-frequency shifts. The near agreement between our model and experiments confirms the earlier measurement of intrafield distortion. Given this correlation of intrafield distortion with frequency mismatch, we will be able to correct the mismatch by feeding appropriate corrections to the beam-deflection electronics.
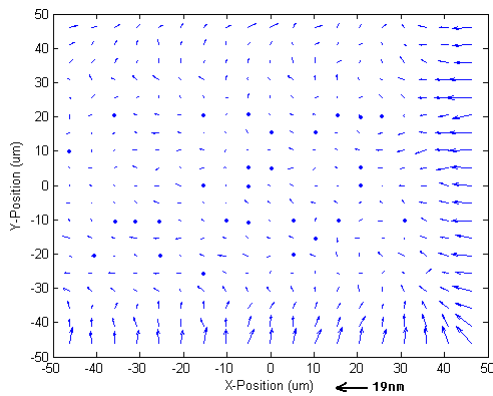
▲ Figure 1: Map of the Raith 150's intrafield distortion in a 100μm deflection Field. The maximum distortion is 19 nm, which is in the lower left corner of the field.
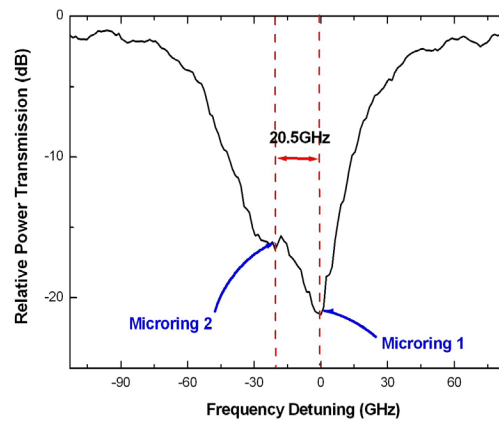
▲ Figure 2: A typical through-port spectrum of a 2nd-order microring filter, with 20.5 GHz frequency mismatch caused by the intrafield distortion.
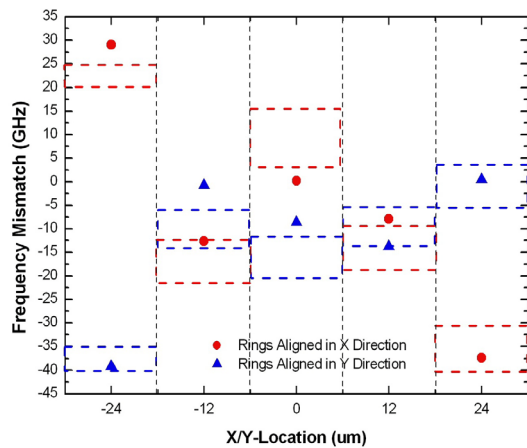
▲ Figure 3: Frequency mismatch of 2nd-order microring resonators. The red dots represent two rings aligned in the X direction, while the blue triangles represent alignment in the Y direction. The boxes with corresponding colors enclose measured frequency mismatches.

Nanometrology

R. Heilmann, Y. Zhao, D. Trumper, M.L. Schattenburg
Sponsorship: NSF

Manufacturing of future nanodevices and systems will require accurate means to pattern, assemble, image and measure nanostructures. Unfortunately, the current state-of-the-art of dimensional metrology, based on the laser interferometer, is grossly inadequate for these tasks. While it is true that when used in carefully-controlled conditions interferometers can be very precise, they typically have an accuracy measured in microns rather than nanometers. Achieving high accuracy requires extraordinarily tight control of the environment and thus high cost. Manufacturing at the nanoscale will require new technology for dimensional metrology that enables sub-1-nm precision and accuracy in realistic factory environments.

A recently formed MIT-UNC–Charlotte team is developing new metrology technology based on large-area grating patterns that have long-range spatial-phase coherence and ultra-high accuracy. Our goal is to reduce errors in gratings by 10-100 times over the best available today. These improved gratings can be used to replace interferometers with positional encoders to measure stage motion in a new nanomanufacturing tools and to calibrate the dimensional scales of existing nanofabrication tools. This increased precision and accuracy will enable the manufacturing of nanodevices and systems that are impossible to produce today. Improved dimensional accuracy at the nano-to-picometer scale will have a large impact in many nanotechnology disciplines including semiconductor manufacturing, integrated optics, precision machine tools, and space research.

As part of this effort, we will utilize a unique and powerful tool recently developed at MIT called the Nanoruler that can rapidly pattern large gratings with a precision well beyond other methods. Another unique high-precision tool, the UNCC-MIT-built Sub-Atomic Measuring Machine (SAMM), is being brought to bear to research new ways to quantify and reduce errors in the gratings. Recent work at MIT focuses on improving the thermal controls in the Nanoruler lithography enclosure and developing an improved interferometer system to reduce errors in the stage metrology frame. At UNCC the SAMM is undergoing extensive refurbishment and improvements designed to boost accuracy of the interferometer.
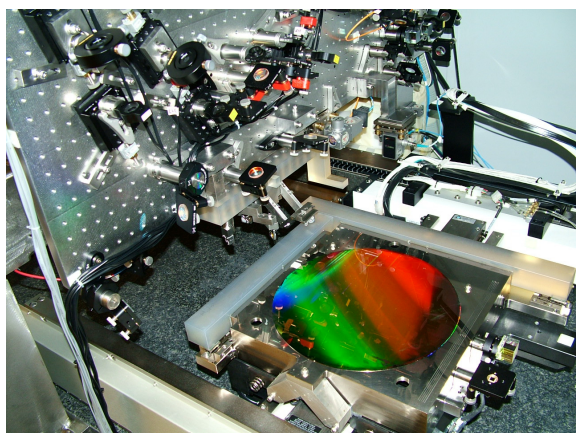
▲ Figure 1: Photograph of the Nanoruler lithography and metrology system built by MIT students. This unique tool is the most precise grating patterning and metrology system in the world.
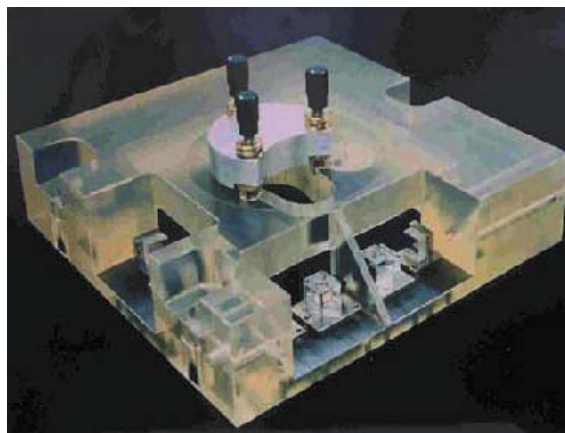
▲ Figure 2: Photograph of reference block/sample holder for the Sub-Atomic Measuring Machine at the University of North Carolina – Charlotte.

References

[1]   P. Konkola, C. Chen, R.K. Heilmann, C. Joo, J. Montoya, C.-H. Chang, and M.L. Schattenburg, "Nanometer-level repeatable metrology using the Nanoruler," *Journal of Vacuum Science Technology B*, vol. 21, pp. 3097-3101, 2003.
[2]   R.K. Heilmann, C.G. Chen, P.T. Konkola, and M.L. Schattenburg, "Dimensional metrology for nanometer-scale science and engineering: Towards sub-nanometer accurate encoders," *Nanotechnology*, vol. 15, pp. S504-S511, 2004.
[3]   J. Montoya, R.K. Heilmann, and M.L. Schattenburg, "Measuring two-axis stage mirror non-flatness using linear/angular interferometers," *Proc. of the 19th Annual Meeting of the American Society for Precision Engineering*, 2004, vol. 34, pp. 382-385.
[4]   Y. Zhao, D.L. Trumper, R.K. Heilmann and M.L. Schattenburg, "Optimization and temperature mapping of an ultra-high thermal stability environmental enclosure," *Journal of Precision Engineering*, 2007, to be published.

Microscopy Beyond the Diffraction Limit Using Absorbance Modulation

H.Y. Tsai, R. Menon, H.I. Smith
Sponsorship: Deshpande Center for Technological Innovation

Absorbance Modulation Imaging (AMI) is an approach to overcome the optical diffraction limit in the far–field, thereby achieving macro-molecular resolution with photons. Preliminary experiments show promising results that agree well with theoretical predictions [1].

AMI relies on an absorbance-modulation layer (AML), composed of photochromic molecules. Illumination at one wavelength, λ_2, renders the AML opaque, while illumination at a shorter wavelength, λ_1, renders it transparent. When illuminated with a ring-shaped spot at λ_2 co-incident with a focused spot at λ_1, the dynamic competition results in a nanoscale aperture, through which λ_1 can penetrate to the substrate beneath. The size of the aperture is limited only by the photo-kinetic parameters of the AML, and the intensity ratio of the two illuminating wavelengths, not the absolute intensities [2]. By scanning this dynamic nanoscale aperture over the sample, resolution beyond the far-field diffraction limit is achieved. A related technique was demonstrated in stimulated-emission-depletion (STED) fluorescence microscopy [3]. However, while STED requires high power pulsed illumination and fluorescent markers, AMI can operate at low illumination intensity. A schematic of an AMI microscope is shown in Figure 1. Collimated lights at λ_1 and λ_2 illuminate the *dichromat*, a binary phase element, which creates a ring-shaped spot at λ_2 and a round spot at λ_1. Figure 2 shows the phase transmission function of a dichromat and the intensity distributions in its focal plane for the two wavelengths.
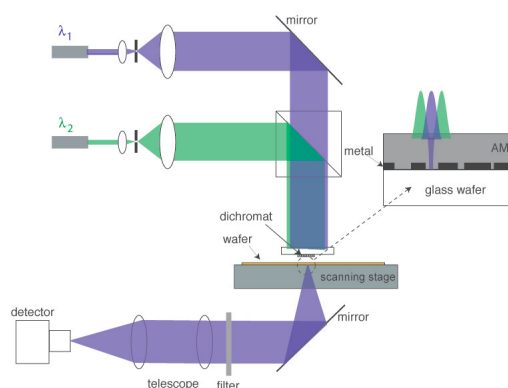
▲ Figure 1: Schematic of absorbance-modulation imaging (AMI) microscope. The ring illumination at λ2 creates a local subwavelength aperture for λ1 in the AML through which the underlying object is illuminated and the scattered light collected. Multiple dichromats generate separate signals enabling parallelism and enhanced throughput. The inset shows the schematic of a resolution test structure consisting of metal lines on a glass wafer.
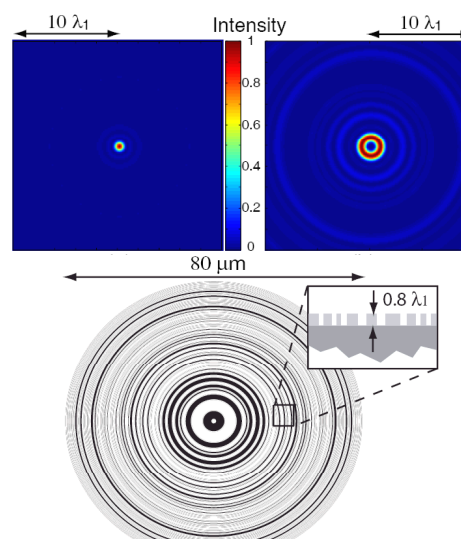
▲ Figure 2: Output light intensity distributions at (a) λ1 = 400nm, (b) λ2 = 532nm, and (c) the phase transmission function of the dichromat. The phase step in this case is 0.8λ1 as shown in the inset of (c). The dichromat creates ring-shaped illumination for λ2 and a focal spot for λ1.

References

[1] R. Menon, H-Y Tsai, and S.W. Thomas III, "Far-field generation of localized light fields using absorbance modulation," *Physical Review Letters*, vol. 98, no. 4, pp. 043905, Jan. 2007.

[2] R. Menon and H.I. Smith, "Absorbance modulation optical lithography," *Journal of the Optical Society of America A*, vol. 23, no. 9, pp. 2290-2294, Sept. 2006.

[3] S.W. Hell and J. Wichmann, "Breaking the diffraction resolution limit by stimulated emission: Stimulated-emission-depletion fluorescence microscopy," *Optics Letters*, vol.19, no. 11, pp. 780-782, June 1994.

# Nanofabricated Reflection and Transmission Gratings

M. Ahn, C.-H. Chang, R.K. Heilmann, Y. Zhao, M.L. Schattenburg

Diffraction gratings and other periodic patterns have long been important tools in research and manufacturing. Diffraction is due to the coherent superposition of waves—a phenomenon with many useful properties and applications. Waves of many types can be diffracted, including visible and ultraviolet light, x-rays, electrons, and even atom beams. Periodic patterns have many useful applications in fields such as optics and spectroscopy; filtering of beams and media; metrology; high-power lasers; optical communications; semiconductor manufacturing; and nanotechnology research in nanophotonics, nanomagnetics, and nanobiology.

Diffraction gratings can be divided into reflection gratings, which use diffracted waves on the same side as the incident waves, and transmission gratings, which use waves that are transmitted through the grating. Both have their strength and weaknesses, depending on the application. A long-standing problem with transmission gratings is the strong absorption of extreme-ultraviolet (EUV) and soft x-ray photons upon transmission, and thus a low diffraction efficiency in this important wavelength band. We have recently solved this problem with the invention and fabrication of critical-angle trans-

mission (CAT) gratings. This new design for the first time combines the high broadband efficiency of blazed grazing-incidence reflection gratings [1] with the superior alignment and figure tolerances, and the low weight of transmission gratings [2]. CAT gratings consist of ultrahigh aspect ratio, nm-thin freestanding grating bars with sub-nm smooth sidewalls that serve as efficient mirrors for photons incident at graze angles below the angle for total external reflection (see Figures 1 and 2). Most photons are not absorbed since they propagate only through vacuum. Blazing can concentrate diffracted power into a single or a few desired diffraction orders. Blazing also enables the use of higher diffraction orders and leads to manifold increases in spectral and spatial resolution in spectrometer or focusing applications, respectively.

Fabrication of these challenging structures is described in [3]. X-ray tests on a 574-nm-period prototype have shown outstanding > 50% and > 30% on-blaze diffraction efficiency in the 17-49-nm- and 2.75–10.6-nm-wavelength bands, respectively. Shorter period gratings will provide higher efficiency at shorter wavelengths.
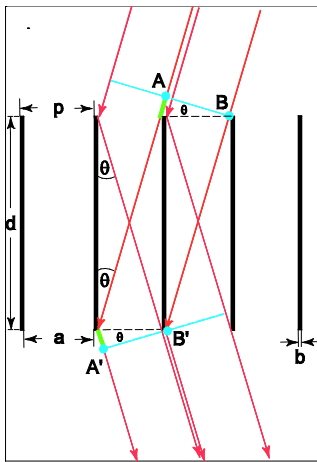
▲ Figure 1: Schematic of the CAT grating principle. Diffraction peaks appear where the path length difference AA'-BB' equals an integer multiple of the wavelength.
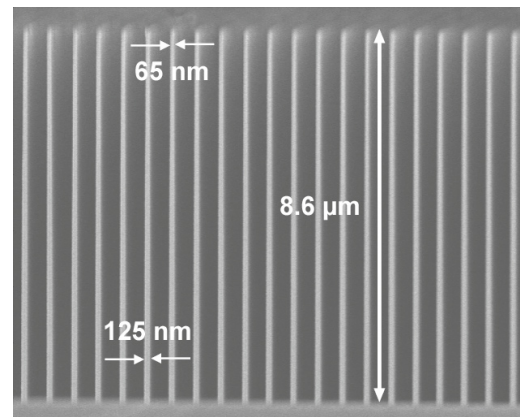
▲ Figure 2: Scanning electron micrograph of a cleaved cross section through a 574-nm-period silicon CAT grating that was (intentionally) not etched all the way through. The grating bar aspect ratio is close to 100 and is increased to ~ 150 for the final grating.

References

[1] J.F. Seely, L.I. Goray, B. Kjornrattanawanich, J.M. Laming, G.E. Holland, K.A. Flanagan, R.K. Heilmann, C.-H. Chang, M.L. Schattenburg, and A.P. Rasmussen, "Efficiency of a grazing-incidence off-plane grating in the soft x-ray region," *Applied Optics*, vol. 45, no. 8, pp. 1680-1687, Mar. 2006.

[2] K. Flanagan, M. Ahn, J. Davis, R.K. Heilmann, D. Huenemoerder, A. Levine, H. Marshall, G. Prigozhin, A. Rasmussen, G. Ricker, M.L. Schattenburg, N. Schulz, and Y. Zhao, "Spectrometer concept and design for x-ray astronomy using a blazed transmission grating," *Proc. SPIE*, vol. 6688, 66880Y, pp. 1-12, Sept. 2007.

[3] M. Ahn, R.K. Heilmann, and M.L. Schattenburg, "Fabrication of ultrahigh aspect ratio freestanding gratings on silicon-on-insulator wafers," *Journal of Vacuum Science and Technology B*, vol. 25, no. 6 , pp. 2593-2597, Nov. 2007.

Templated Self-Assembly of Sub-10-nm Quantum Dots

J. Leu, B. Cord, P. Anikeeva, J. Halpert, M. Bawendi, V. Bulović, K.K. Berggren
Sponsorship: SRC/FCRP MSD, NRI, IBM

Patterned templates can guide the self-assembly of nanoparticles into ordered arrays [1]. Our motivation in pursuing templated self-assembly is to develop a robust method for the creation of ordered structures at length scales below ten nanometers. The basic process entails creating surface relief templates via electron-beam lithography and spin-coating a suspension of colloidal nanoparticles onto the template. As the solvent evaporates, the quantum dots self-assemble primarily through the capillary forces created by the dewetting of the template [2].

We demonstrated this technique at sub-10-nm-length scales by spin-coating a solution of organically-capped CdZnS semiconducting quantum dots onto nanopatterned grating structures on silicon substrates. We observed the geometric confinement of the quantum dots via physical templating and capillary forces into well-ordered monolayer aggregates with defined lattice orientations. While recent research has demonstrated the ability to self-assemble sub-10-nm metallic nanoparticles via capillary forces into physical templates of similar size [2], this work is unique in the demonstration of lattice orientation control via physical templating at sub-10-nm-length scales.
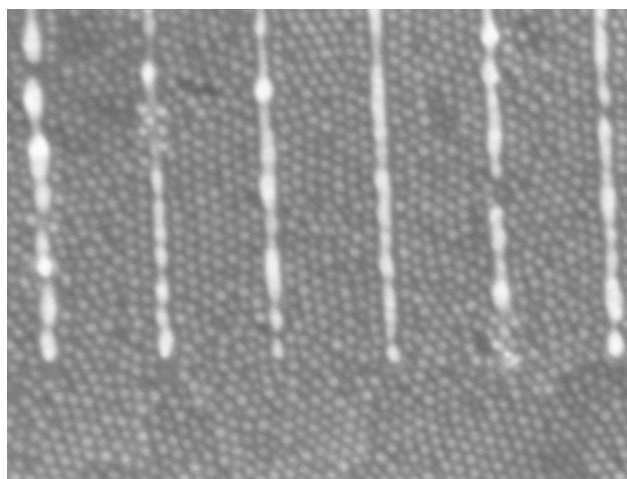
▲ Figure 1: Scanning electron micrograph of a self-assembled quantum dot monolayer on a templated silicon substrate. The vertical lines visible are part of a template grating, with 10-nm-wide, Au lines with height varying from 20-80 nm at a pitch of 80 nm. The spheres are organically capped 8-nm CdZnS semiconducting quantum dots.

References
[1] Y. Yin, Y. Lu, B. Gates, and Y. Xia, "Template-assisted self-assembly: A practical route to complex aggregates of mondispersed colloids with well-defined sizes, shapes, and structures," *Journal of the American Chemical Society*, vol. 123, pp. 8718-8729, 2001.
[2] J.A. Liddle, Y. Cui, and P. Alivisatos, "Lithographically directed self-assembly of nanostructures," *Journal of Vacuum Science and Technology B*, vol. 22, no. 6, pp. 3409-3414, Nov./Dec. 2004.

Hydrogen Silsesquioxane Nano-posts as Decoys for Guiding the Self-assembly of Block Copolymers

J.K.W. Yang, Y.S. Jung, I. Bita, E.L. Thomas, C.A. Ross, K.K. Berggren
Sponsorship: MIT

According to the International Technology Roadmap for Semiconductors, semiconductor companies are expected to produce memory cells with a half-pitch of 22 nm by the year 2011. Fabricating such small structures is a huge challenge even with today's most advanced photolithography methods. However, the technology for making sub-20-nm nanostructures is already available in the self-assembly of block-copolymers (BCP). This bottom-up technique is scalable to even smaller dimensions by choosing tinier BCP molecules, making it an attractive "next-generation lithography" method for creating dense periodic structures over large areas. Major challenges still remain in (1) the accurate control of the order and position of the nanostructures, and (2) the formation of arbitrary structures using BCPs. In this work, we focus on solving the first problem.

Figure 1 shows the randomly oriented, hexagonally-packed nanostructures formed in a BCP film on a flat Si substrate. This pattern was formed after annealing a thin layer of polystyrene-b-polydimethylsiloxane (PS-b-PDMS) BCP and selective etching of the PS majority block [2]. These nanostructures that lack order have limited use as most applications such as bit-patterned media require long-range order. To induce long-range order in the BCP, we first introduced topography on the flat surface by fabricating a periodic array of posts in hydrogen silsesquioxane (HSQ) resist by electron-beam lithography (see Figure 2a). These posts, ~10 nm in diameter and 35 nm tall, acted as decoys (or substitutes) for single BCP spheres. Figure 2b shows that order and orientation control were achieved when the BCP self-assembled about the array of posts. In contrast to previous work [1] where the topographical structures (e.g., trenches) used for guiding the BCP were large and clearly identifiable after processing, our nano-posts blend in among the BCP spheres while physically pinning down the BCP lattice position in 2D. As a result, the template of posts allows efficient use of the surface area of the substrate.

Adjusting the lattice spacing of the HSQ posts produced formation of different BCP packing orientations that were commensurate with the HSQ lattice. We therefore have control over the packing order and orientation of the BCP spheres. The resultant PDMS and HSQ nanostructures were etch-resistant and could be used for pattern transfer into underlying functional materials such as magnetic films for high-density data storage applications.
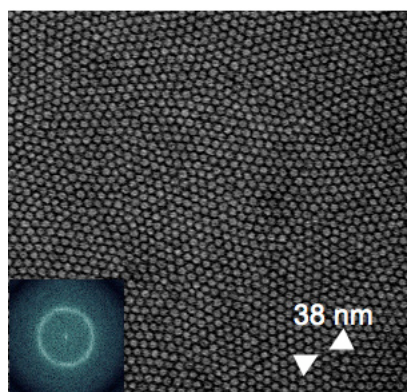
▲ Figure 1: SEM image of randomly oriented spheres formed by BCP self-assembly on a flat surface. The Fourier transform (inset) shows a circular halo characteristic of randomly oriented grains.
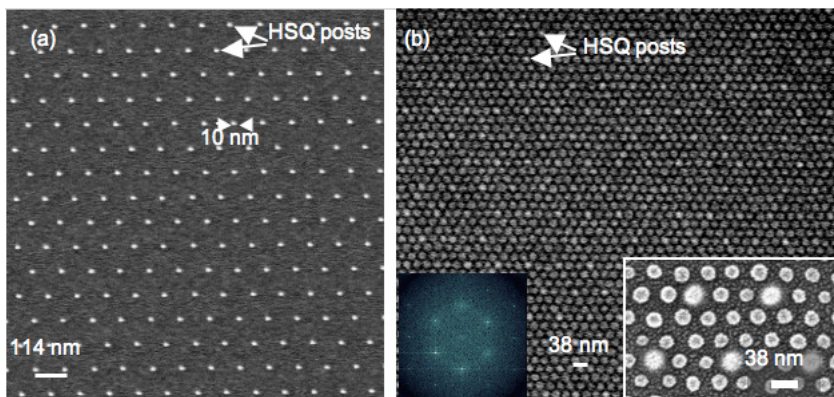
▲ Figure 2: (a) SEM image of a periodic array of 35-nm-tall, 10-nm-diameter HSQ posts fabricated by electron-beam lithography and developed in a high-contrast salty developer [3]. b) Ordered packing of BCP spheres guided by the lattice of HSQ posts. HSQ posts blend in with the BCP spheres but are visible as slightly brighter dots in the image and bottom-right inset. The Fourier transform (left inset) shows an arrangement of bright spots characteristic of a hexagonally packed crystal.

References

[1] J.Y. Cheng, A.M. Mayes, and C.A. Ross, "Nanostructure engineering by templated self-assembly of block copolymers," *Nature Materials*, vol. 3, no, 11, pp. 823-828, Nov. 2004.

[2] Y.S. Jung and C.A. Ross, "Orientation-controlled self-assembled nanolithography using a polystyrene-polydimethylsiloxane block copolymer," *Nano Letters*, vol. 7, no. 7, pp. 2046-2050, July 2007.

[3] J.K.W. Yang and K.K. Berggren, "Using high-contrast salty development of hydrogen silsesquioxane for sub-10-nm half-pitch lithography," *Journal of Vacuum Science & Technology B*, vol. 25, no. 6, pp. 2025-2029, Nov. 2007.

Templated Self-assembly of Block Copolymers for Nanolithography

C.A. Ross, H.I. Smith, K.K. Berggren, E.L. Thomas, F. Ilievski, V. Chuang, Y.S. Jung
Sponsorship: NSF, CMSE, Singapore-MIT Alliance, SRC

Self-organized macromolecular materials can provide an alternative pathway to conventional lithography for the fabrication of devices on the nanometer scale. In particular, the self-assembly of the microdomains of diblock copolymers within lithographically-defined templates to create patterns with long-range order has attracted considerable attention, with the advantages of cost-effectiveness, large area coverage, and compatibility with pre-established top-down patterning technologies. Block copolymers consist of two covalently bound polymer chains of chemically distinct polymer materials. The chains can self-assemble to form small-scale domains whose size and geometry depend on the molecular weights of the two types of polymer and their interaction [1]. On the one hand, with the purpose of fabricating arrays of magnetic nanosized dots, which are a potential candidate for magnetic hard-drive media, we are working on templating the block copolymers in a removable template. Previously, sphere-forming polystyrene-b-ferrocenyldimethylsilane (PS-PFS) diblock copolymers were successfully aligned

in 2-D [2] or 3-D [3] templates. On the other hand, cylindrical morphology of block copolymers can be used for defining nanoscale line patterns, as demonstrated in Figure 1a. Poly(styrene-b-dimethylsiloxane) (PS-PDMS) diblock copolymers have a large interaction parameter and a high etch contrast between two blocks, which are desirable for long-range ordering and pattern-transfer into functional materials [4]. Concentric ring patterns can also be obtained by using circular templates, as shown in Figure 1b. Beyond rather limited morphologies of diblock copolymers, an appropriate combination of block sequence, interaction parameter of the adjacent blocks, volume fraction, and molecular weights of ABC triblock polymer thin films provides a diversity of new structures. For example, core-shell structured triblock terpolymer can be obtained by designing the block sequence and volume fraction of the blocks. Figure 2 presents vertically oriented high-density nanorings from PB-PS-PMMA polymers after the selective removal of PB and PMMA and after pattern-transfer onto a SiO_2 film.
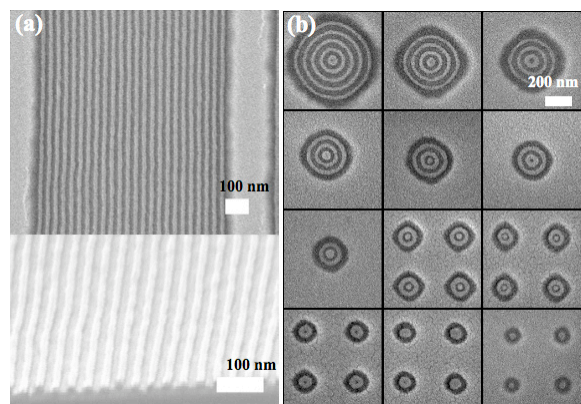
▲ Figure 1: (a) Line patterns from PS-PDMS diblock copolymers under linear confinement and (b) concentric ring patterns under circular confinement

▲ Figure 2: (a) Vertically oriented hollow cylinders of PS from PB-PS-PMMA triblock copolymers. (b) RIngs after CHF_3 RIE for patterning a SiO_2 film.

References

[1]   E.L. Thomas and R.L. Lescanec, "Phase morphology in block copolymer systems," *Philosophical Transactions of the Royal Society A,* vol. 348, pp. 146-164, 1994.
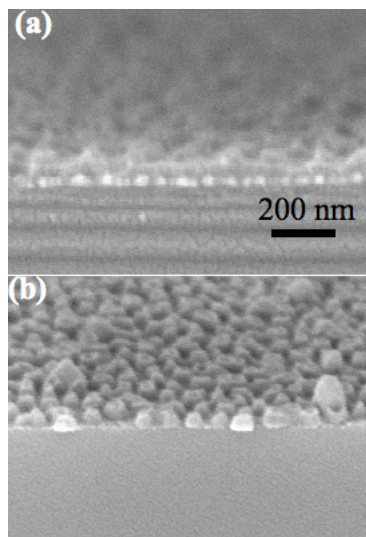[2]   J. Cheng, C.A. Ross, and A. Mayes, "Nanostructure engineering by templated self-assembly," *Nature Materials,* vol. 3, pp. 823-828, 2004.
[3]   V.P. Chuang, J.Y. Cheng, T.A. Savas, and C.A. Ross, "Three-dimensional self-assembly of spherical block copolymer domains into V-shaped grooves," *Nano Letters,* vol. 6, pp. 2332-2337, 2006.
[4]   Y.S. Jung and C.A. Ross, "Orientation-controlled self-assembled nanolithography using a polystyrene-polydimethylsiloxane block copolymer," *Nano Letters,* vol. 7, no. 7, pp. 2046-2050, June 2007.

Building Three-dimensional Nanostructures via Membrane Folding

W.J. Arora, A.J. Nichol, G. Barbastathis, H.I. Smith

In Nanostructured Origami[1] thin membranes are patterned in 2D and are then automatically folded in sequence to produce a 3D configuration. We have developed methods of both folding actuation and folded-structure alignment for patterned silicon-nitride membranes. We have demonstrated that ion implantation can be used to fold membranes. Figure 1 shows data from membranes implanted with high doses of helium. The implanted ions create stress, forcing the membrane to bend. A minimum bend radius of 1 μm using 100 nm-thick silicon nitride was achieved. The resulting 3D structure remains folded unless heated above 400C, at which point the helium diffuses out and the structure unfolds. In addition to experimental demonstration, we model the physics of the ion implantation to show that the ion-implant profile correlates to the observed folding. This is most clearly evidenced by the fact that membranes given low energy (shallow depth) implants fold downwards while membranes given high energy (large depth) implants fold upwards. Magnetic forces are an alternate actuation method to fold, and to align and reconfigure nanopatterned membranes.[2] After fold-ing, the membranes accurately self-align when brought into close proximity due to the interactive magnetic force between the arrays of nanomagnets. Since the self-alignment accuracy is better than the lithographic resolution, the membranes may be self-aligned to nanometer precision. We are also developing a nanomagnetic step-per that utilizes the force between arrays of nanomagnets to precise-ly move a nanopatterned membrane along a substrate. After folding and magnetically aligning two membranes, the system is actuated by an external magnetic field that rotates or flips the magnetization of the nanomagnets, thus changing the equilibrium position. Figure 2a shows a micromagnetic simulation of a bi-stable switcher that changes between two positions by rotating the external field. Figure 2b shows a schematic of the nanomagnet switcher, which uses cir-cular nanomagnets that shift one step per full rotation of the exter-nal magnetic field. The stepper is wirelessly controlled and is non-hysteretic so the need for feedback is eliminated. We are exploring the stepper's use for reconfigurable photonic systems and wireless nano-device control.
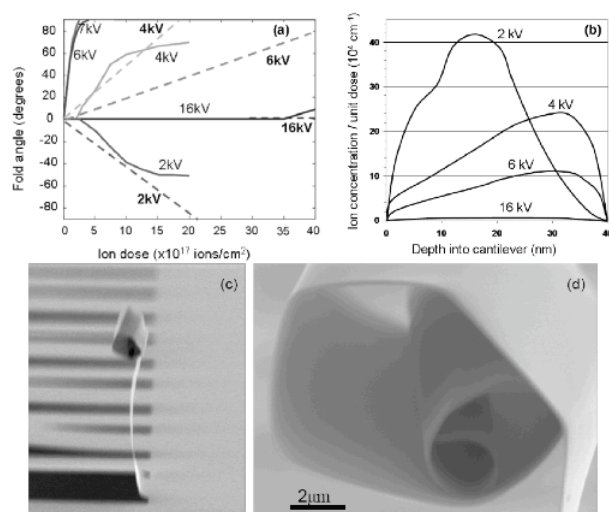
▲ Figure 1: a) Fold angle vs dose for different 40-nm-thick silicon nitride cantilevers implanted with helium (solid lines are experimental; dashed lines are prediction. b) Corresponding ion profiles within the cantilever. c, d) Experimental demonstration of folding.
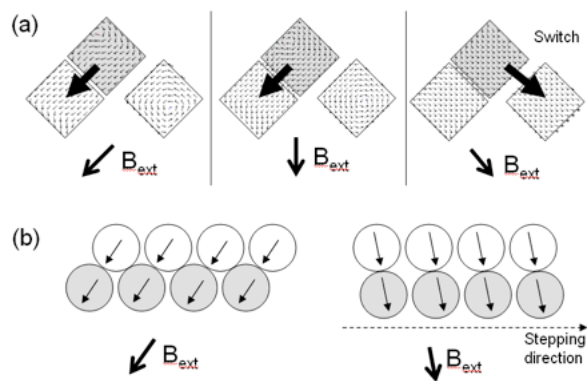
▲ Figure 2: (a) Micromagnetic model of a nanomagnetic switcher. (b) schematic of a nanomagnet stepper motor that moves one period with each full rotation of the external magnetic field.

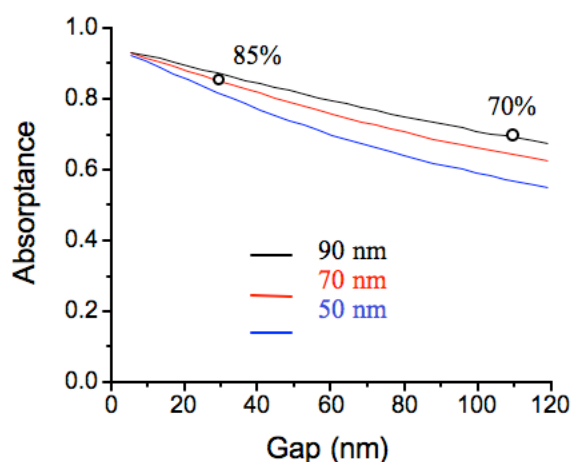## References

[1] H.J. In, W.J. Arora, T. Buchner, S.M. Jurga, H.I. Smith, and G. Barbastathis. *2004 4th IEEE Conference on Nanotechnology (IEEE Cat. No.04TH8757)*, 2004, p 358–60 JVSTB:

[2] A.J. Nichol, Paul S. Stellman, W.J. Arora, George Barbastathis. "Two-step magnetic self-alignment of folded membranes for 3D nanomanufacturing." Accepted: *Journal of Microelectronics Engineering*, Dec. 2006.

Fabrication of Superconducting Nanowire Single-photon Detectors with High Fill-factors

J.K.W. Yang, A.J. Kerman, V. Anant, E.A. Dauler, K.K. Berggren
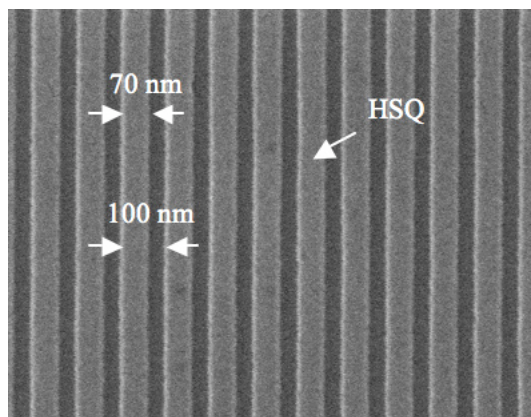Sponsorship: AFOSR, MIT

In the past, we have fabricated superconducting nanowire single-photon detectors (SNSPDs) with detection efficiencies (DE) as high as 57% at 1550-nm wavelengths [1]. The nanowires in these SNSPDs were 90 nm wide and were separated by 110 nm (i.e., a 45% fill factor) in a meander structure patterned in NbN films. While a 57 % DE is acceptable for many applications, a much higher DE will be valuable (if not necessary) in certain applications such as linear-optics quantum computing and photon number resolution. One approach to increasing the DE of SNSPDs is to increase the optical absorption of the device by increasing the fill factor of the meander structure.

Figure 1 shows numerical calculations of the absorptance in the SNSPD meander structure, indicating that reducing the gap width between wires in the meander can significantly increase photon absorptance and hence the DE. For example, we can predict that by increasing the fill factor from the current value of 45% to 70%, we would increase the device DE from 57% to ~70%.

Recently we developed a high-resolution nanofabrication method using a combination of a high-contrast resist process and electron-beam lithography to achieve sub-10-nm nanostructure dimensions [2]. This technique could be used to fabricate SNSPDs with fill factors as high as 80 % and wire widths as narrow as 40 nm. Figure 2 shows an example of a grating structure with 70% fill factor that has been fabricated in HSQ resist using this method.

▲ Figure 1: Numerical calculations show that the photon absorptance in the SNSPD meander increases with decreasing gap width between the nanowires. Our original SNSPD design of 90-nm-wide wire with a 110-nm-wide gap has an absorptance of ~70%. However, increasing the fill factor through better lithography to achieve 70-nm-wide wires and a gap width of 30 nm will result in an increase in absorptance to 85%, leading to higher detection efficiencies.

▲ Figure 2: Top-down SEM image of HSQ structures on Si with a fill factor of 70%, which could potentially be used for making SNSPDs with higher DE.

References
[1] K.M. Rosfjord, J.K.W. Yang, E.A. Dauler, A.J. Kerman, V. Anant, B.M. Voronov, G.N. Gol'tsman, and K.K. Berggren, "Nanowire single-photon detector with an integrated optical cavity and anti-reflection coating," *Optics Express*, vol. 14, no. 2, pp. 527-534, Jan. 2006.
[2] J.K.W. Yang and K.K. Berggren, "Using high-contrast salty development of hydrogen silsesquioxane for sub-10-nm half-pitch lithography," *Journal of Vacuum Science & Technology B*, vol. 25, no. 6, pp. 2025-2028, Nov. 2007.

# Carbon Nano-Switches for Low-leakage Circuit Applications

K.M. Milaninia, C.E. Schmitt, A.I. Akinwande, M.A. Baldo, A.P. Chandrakasan
Sponsorship: SRC/FCRP IFC, DARPA

Nanoelectromechanical switches (NEMS) exhibit minimal leakage current in the off state. Consequently, they may find application in low-power electronics. This work focuses on the fabrication of a vertically oriented nano-switch using a carbon fiber or nanotube as the active component. Figure 1 shows the device schematic, and Figure 2 shows an SEM image of the self-aligned fabrication process used to create the nano-switch [1]. The device consists of a carbon nanotube/fiber grown directly on a highly doped silicon substrate between two contacts that are electrically isolated from the substrate by an insulator. The device is actuated when a voltage is applied between the substrate and one of the contacts. This voltage causes the nanotube to be pulled into and eventually make physical contact with one of the contacts, which allows current to flow between the substrate and the contact.

One of the primary benefits of the nano-switch is that it has extremely low leakage current because a physical gap separates the nanotube from the contact during the off state. One possible application that takes advantage of the reduced leakage is power-gating idle circuit blocks. The nano-switch is connected as a header switch between the power supply and the load circuit. During normal operation, the nano-switch acts as a short circuit and power is supplied to the load circuit. When the circuit is not in use, the nano-switch is opened and the supply voltage is disconnected to reduce power consumption. This technique is similar to power-gating with a high threshold CMOS device, but the nano-switch provides extra power savings because it has even less leakage current.

A test chip has been designed to quantify the power savings of the nano-switch for this power-gating application. The chip also implements proof-of-concept SRAM and reconfigurable interconnect circuits that explore other potential benefits of the nano-switch.
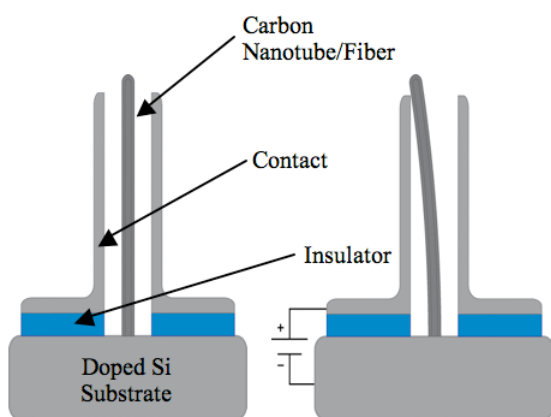
▲ Figure 1: Left) Schematic of a vertically oriented carbon nano-switch. Right) Carbon nano-switch upon actuation using an applied voltage between the substrate (i.e., tube) and a contact.
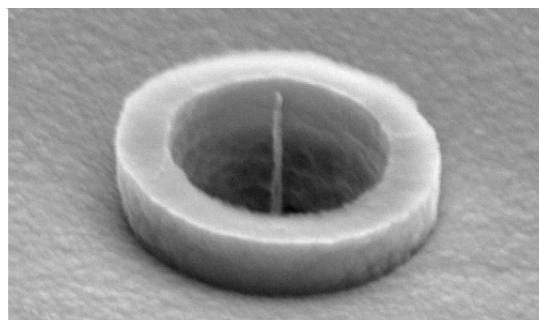
▲ Figure 2: An SEM image of a carbon nano-based field-emitter produced by the self-aligned fabrication process [1].

Reference

[1]   L.-Y. Chen, L.-F. Velasquez-Garcia, X. Wang, K. Teo, and A.-I. Akinwande, "A micro ionizer for portable mass spectrometers using double-gated isolated vertically aligned carbon nanofiber arrays," *International Electron Devices Meeting*, pp. 843-846, Dec. 2007.

Magnetic Nanostructures for Data Storage

Y. Oh, M. Ciria, D. Navas, F. Ilievski, V.P. Chuang, C.A. Ross
Sponsorship: Fulbright Fellowship, NSF

We are investigating the fabrication and magnetic properties of various types of magnetic nanostructures made using non-conventional lithography and self-assembly processes, for applications in patterned magnetic recording media and other data storage devices. In one set of experiments, we use block copolymer lithography to pattern arrays of magnetic "dots" with perpendicular anisotropy [1]. The dots form arrays with periodicity of 30 – 50 nm and the magnetization of each dot can point up or down, to represent one bit of data. By investigating the thermally activated reversal process, we can show that the dots switch independently and coherently, which is desirable for a patterned recording medium. The block copolymer can be templated using surface relief to create arrays with long range order (Figure 1).

We have also examined the formation of periodic arrays of Co nanoparticles by the templated dewetting of a Co film deposited over a substrate with inverted pyramidal pits etched into it. The dewetting, achieved by a high temperature anneal, produces a uni-

form array of Co particles (Figure 2) with an f.c.c. crystal structure and consequently low magnetic anisotropy. This process is now being explored for other magnetic alloys. Another self-assembly process that can be used to form magnetic arrays is the use of anodic alumina films, which are created from aluminum metal by anodization, and which contain ordered arrays of pores that can be used as templates to form arrays of magnetic nanowires [2].

Finally, we have investigated the magnetic properties of narrow lines patterned from a single-crystal epitaxial Cu/Ni/Cu film using interference lithography. The Ni film is highly strained, and as a result it develops a magnetization perpendicular to the film plane. Patterning the film relieves stress and leads to stripes with an in-plane magnetization that is perpendicular to the stripe length – an unusual magnetization orientation.
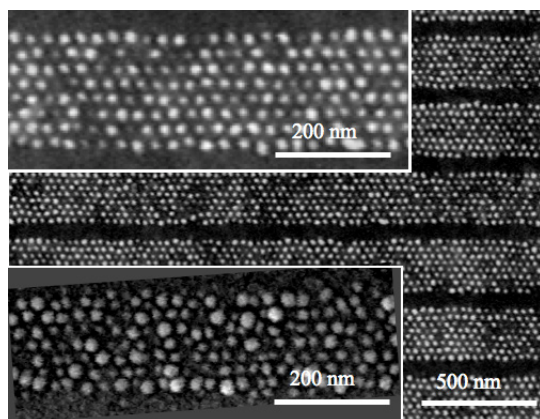
▲ Figure 1: Top inset and background: Scanning electron micrographs of an array of W dots on a CoCrPt perpendicular-anisotropy film. The W dots were made using a block copolymer that had been ordered into rows using a removable topographic template. Bottom inset: An array of magnetic dots formed by using the W dots as an etch mask for patterning the CoCrPt with Ne ion-beam etching.
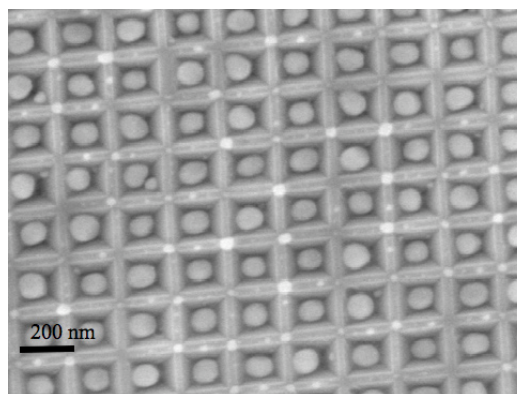
▲ Figure 2: Array of Co nanoparticles formed within 200-nm-period pits etched in a silicon substrate. The 15-nm as-deposited film was dewetted by annealing at 850˚ C in a reducing atmosphere.

References
[1]   F. Ilievski, C.A. Ross, and G.J. Vancso, "Magnetic reversal phenomena of perpendicular magnetic islands fabricated by block copolymer lithography," *Journal of Applied Physics*, vol. 103, no. 7, pp. 07C520:1-3, Apr. 2008.
[2]   D. Navas, K.R. Pirota, P. Mendoza Zelis, D. Velazquez, C.A. Ross, and M. Vazquez, "Effects of the magnetoelastic anisotropy in Ni nanowire arrays," *Journal of Applied Physics*, vol. 103, no. 7, pp. 07D523:1-3, Apr. 2008.

Organic Floating-gate Memory Devices

H. Abdu, S. Paydavosi, O.M. Nayfeh, D.A. Antoniadis, V. Bulović
Sponsorship: SRC/FCRP MSD

Conventional non-volatile flash memories face obstacles to continued scaling, such as the inability to use thinner tunneling oxides and poor charge retention due to defects in the tunneling oxide [1]. A possible solution is to replace the continuous floating gate, where the charge is stored, with a segmented charge storage film, so that defects in the structure would affect only a few of the many segments that comprise the floating gate [2]. From our earlier work on nanocrystal thin films as floating gates, we established the need for the smallest possible segmented structures, which led us to the use of organic films as floating gates in non-volatile flash memories. As an example, a single organic molecule of 3,4,9,10 –parylene tetra-carboxylic dianhydride (PTCDA) occupies 1 nm^2 in area and is capable of storing and retaining a single charge. A thin film of PTCDA molecules would therefore provide 10^{14} distinct charge storage sites per cm^2, a remarkably high number of storage sites, even when we take into account the fact that only a few percent of these would be occupied when the floating gate is charged. If a defect were present in the tunneling oxide below the floating gate, only a few discreet molecules of PTCDA would be affected due to poor lateral conduction between PTCDA molecules. We can, therefore, project that such a molecular thin film of PTCDA is likely to meet the demanding size and packing density requirements of the advancing flash memory technology.

To demonstrate charge retention in an organic thin film, we construct an organic floating gate capacitor, shown in Figure 2 (inset), by depositing 4 nm of PTCDA as the floating gate. As for the gate dielectric, SiO$_2$ was deposited using Plasma Enhanced CVD (PECVD), which allowed for low temperature oxidation and minimal damage to the organic film below. This capacitor structure is a first step to demonstrating a floating-gate memory cell, as it proves significant in understanding the organic molecular film's ability to be written (charged), erased (discharged), and read (retain charge).

Figure 1 demonstrates the functionality of the organic floating gate capacitor. The capacitance voltage (C-V) plot exhibits hysteresis, which indicates the flatband voltage shift that exists due to charge storage. Also, as Figure 2 shows, the device performs well in endurance tests, withstanding over 300,000 program/erase cycles without much deterioration in the flatband voltage shift.

This initial set of data signifies the potential for organic floating-gate memories as an advancement of flash memory devices. With the scaling enabled by the nano-segmented molecular floating gate, this technology has the potential to achieve **higher memory density,** decreased **power consumption, and increased read/write/erase** speeds, all of which are important benchmarks for future non-volatile memory devices [3].
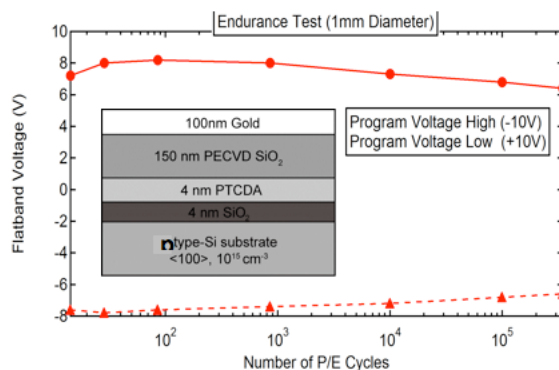

▲ Figure 1: C-V plot of several organic floating-gate capacitors with characteristic hysteresis. Electron charging at -10V and hole charging at +10V.

▲ Figure 2: Schematic diagram of an organic floating-gate capacitor (subset). Endurance test demonstrating over 300,000 program/erase cycles without significant loss in device performance.

References

[1] K. Kinam, "Technology for sub-50nm DRAM and NAND flash manufacturing," *International Electronic Devices Meeting*, 1609340, pp. 323-326, Dec. 2005.
[2] O. Nayfeh, D. Antoniadis, K. Mantey, and M. Nayfeh, "Memory effects in metal-oxide-semiconductor capacitors incorporating dispensed highly monodisperse 1-nm silicon nanoparticles," *Applied Physics Letters*, vol. 90, p. 153105, 2007.
[3] P. Pavan, R. Bez, P. Olivo, and E. Zanoni, "Flash memory cells--an overview," *Proc. IEEE*, vol. 85, no. 8, Aug. 2007, pp. 1248-1271.

Uniform Delivery of Si Nanoparticles on Device-quality Substrates for Nonvolatile Memory Applications Using Spin-coating from Isopropyl Alcohol Colloids

O.M. Nayfeh, D.A. Antoniadis, K. Mantey, M.H. Nayfeh
Sponsorship: SRC/FCRP MSD, Singapore-MIT Alliance, Intel Fellowship

Colloidal dispersions of as-prepared hydrogen-terminated silicon nanoparticles of predominately 2.9 nm in diameter in isopropyl alcohol are spin-coated directly on device-quality thermally grown silicon-dioxide (SiO_2) layers across the entire 150-mm substrates. Atomic force microscopy (AFM) is used to image the nanoparticle distributions and low levels of agglomeration with some signs of nanoparticle ordering are observed. The AFM depth profiling of the nanoparticle size is in agreement with independent high-resolution transmission electron microscopy (HRTEM) measurements. Hartree Fock (HF)-based atomistic simulations confirm the possible formation of Si nanoparticle/isopropanol complexes with a calculated electrostatic binding energy of 30 meV, slightly larger than the room temperature thermal agitation energy. The much-reduced agglomeration can be explained in terms of such complexes that may regulate the inter-nanoparticle and nanoparticle–solvent interactions. The results are of importance for the fabrication of nonvolatile memory devices that use silicon nanoparticles for charge storage.
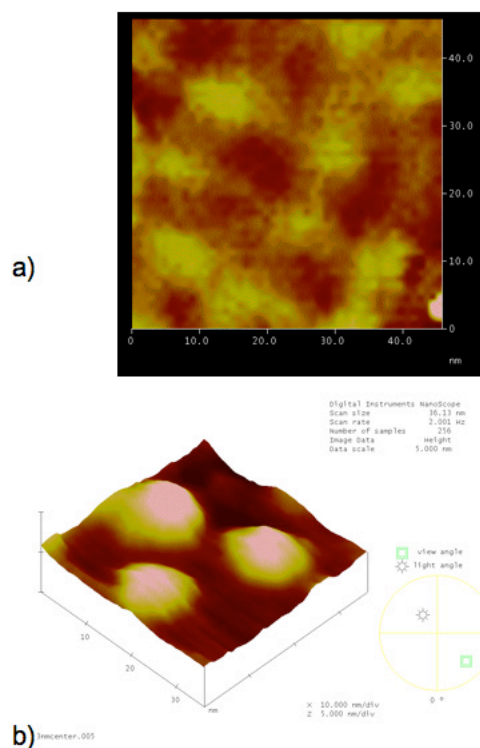
▲ Figure 1: a) Top-view AFM images of silicon nanoparticles in near-array formation on a device-quality thermally grown SiO2 layer. b) Surface-view AFM of silicon nanoparticles. The lateral dimension via AFM is limited by the tip-effect, but AFM resolves the vertical dimension correctly.
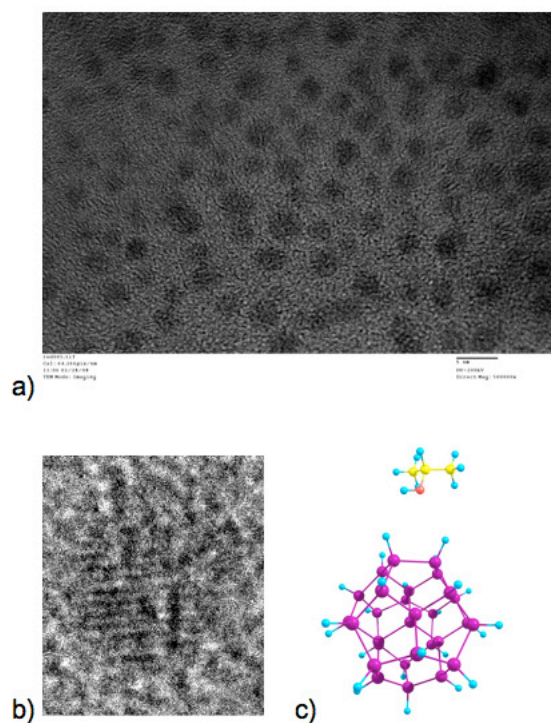
▲ Figure 2: a) High-resolution TEM images of predominately 2.9-nm silicon nanoparticles on a TEM grid showing minimal agglomeration. The size of the nanoparticles is in agreement with the vertical AFM measurements in Figure 1. b) Closeup of single silicon nanoparticle with lattice visible. c) Atomistic simulation structure of a silicon nanoparticle with isopropyl alcohol used for calculation of binding energy.

Reference

[1] O.M. Nayfeh, D.A. Antoniadis, K. Mantey, and M.H. Nayfeh, "Memory effects in metal-oxide-semiconductor capacitors incorporating dispensed highly monodisperse 1 nm silicon nanoparticles,"*Applied Physics Letters*, vol. 90, no. 15, pp. 153105:1–3, Apr. 2007.

Elastic Energy Storage in Carbon Nanotubes

F.A. Hill, T.F. Havel, A.J. Hart, C. Livermore
Sponsorship: Deshpande Center for Technological Innovation, NSERC

The focus of this project is to study the potential of storing energy in the elastic deformation of carbon nanotubes (CNTs) as a step towards lightweight, high-density energy storage. The unique mechanical properties of CNTs, namely a high stiffness of 1 TPa, high strength, high flexibility, and low defect density, make springs made of CNTs a promising medium for elastic energy storage. Theoretical models have shown that CNTs can be stretched reversibly up to 15% [1], while lower strains of up to 6% have been reached experimentally to date [2, 3]. Our initial work has used models to predict the energy density that can be stored in CNTs under different modes of mechanical deformation. The obtainable energy density is predicted to be highest under tensile loading, with an energy density in the springs themselves about 1000 times greater than the maximum energy that can be stored in steel springs, and ten times greater than the energy density of lithium-ion batteries. Practical systems will have lower overall stored energy density once the mass and volume of the spring's supporting structure are taken into account, with a maximum achievable overall stored energy density predicted to be comparable to lithium-ion batteries (see Figure 1). Nonetheless, springs made of CNTs offer a number of advantages over conventional energy storage in electrochemical batteries. In addition to their competitive energy density, CNT springs are based on stretching chemical bonds rather than breaking and reforming chemical bonds, so an energy storage medium based on CNT springs has the potential to operate at higher power densities, under harsher conditions, to deeper discharge levels, and through a larger number of charge-discharge cycles without degradation. In addition, CNT springs have significant potential for storing mechanical energy to drive a mechanical load directly.

Our ongoing research focuses on demonstrating energy storage in CNT springs. While energy can be stored with high density in a single carbon nanotube, grouping individual carbon nanotubes into larger assemblies of densely-packed bundles and ropes offers the advantages of storing larger amounts of energy in a single spring and the ability to couple the resulting spring to a macroscopic load. The proposed springs are composed of well-ordered, aligned, densely-packed CNT groupings in order to ensure effective load transfer within the assembly. The starting material for the springs is CNT forests, highly-ordered, vertically aligned arrangements of millimeter length CNTs grown on a substrate (see Figure 2). The resulting springs will be loaded and characterized to investigate how energy density can be maximized using different spring formation techniques.
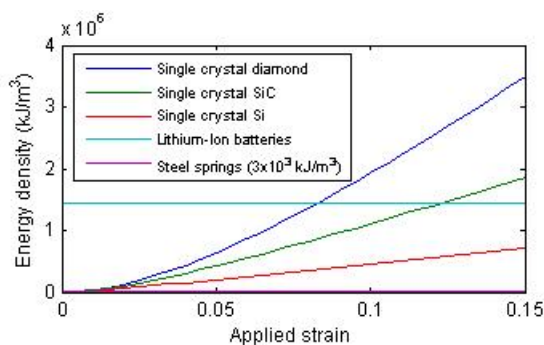
▲ Figure 1: Energy density of CNTs under tensile loading with different support structure materials compared to the energy density of conventional storage technologies.
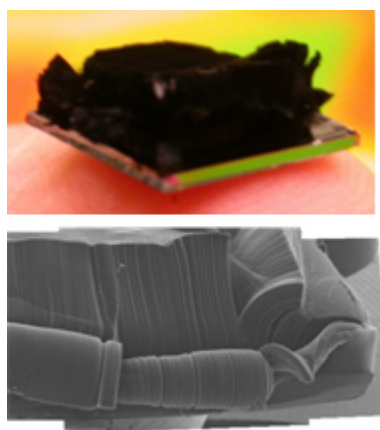
▲ Figure 2: Dense arrays of CNTs in vertically aligned forests [4].

References

[1] M.R. Falvo, G.J. Clary, R.M. Taylor, V. Chi, F.P. Brooks, S. Washburn, and R. Superfine, "Bending and buckling of carbon nanotubes under large strain," *Nature*, vol. 389, no. 12, pp. 582–584, Oct. 1997.

[2] D.A. Walters, L.M. Ericson, M.J. Casavant, J. Liu, D.T. Colbert, K.A. Smith, and R.E. Smalley, "Elastic strain of freely suspended single-wall carbon nanotube ropes," *Applied Physics Letters*, vol. 74, no. 25, pp. 3803–3805, June 1999.

[3] M. Yu, B.S. Files, S. Arepalli, and R.S. Ruoff, "Tensile loading of ropes of single-wall carbon nanotubes and their mechanical properties," *Physical Review Letters*, vol. 84, no. 24, pp. 5552–5555, 2000.

[4] A.J. Hart, L. Laake, and A.H. Slocum, "Desktop growth of carbon nanotube monoliths with in situ optical imaging," *Small*, vol. 3, no. 5, pp. 772-777, 2007.

Nanowire and Thin-film Gas Sensors

K. Sahner, G. Whitfield, Y.S. Jin, H.L. Tuller (in collaboration with I.D. Kim, KIST; A. Rothschild, Technion; J. Lewis, U. Illinois)
Sponsorship: NSF, US-Israel Binational Science Foundation

Gas sensors play a vital role in public health and safety, industrial process control, and in reduction of toxic emissions into the environment [1]. Conductometric gas sensors based on semiconducting metal oxide thin films are of high interest in many applications due to their high sensitivity, small size, and simplicity of measurement. Sensors based on individual nanowires further improve device sensitivity due to the increased area of the chemically active free surface. However, challenges arise due to limited process control and reproducibility during integration of nanowires with conventional microfabrication techniques.

Gas sensors based on interconnected nanowire networks enable improved sensitivity while avoiding typical challenges in integration. The TiO_2 and SnO_2 based nanowire meshes were deposited by collaborators at KIST and U. Illinois onto microfabricated interdigitated electrodes via electrospinning [2] and direct-write [3] techniques. Both techniques enable rapid integration of inorganic nanowire networks with microfabricated structures, via deposition from organic precursor solution (Figure 1). The structures were characterized at MIT over a range of temperatures and gas compositions to confirm high chemical sensitivity (Figure 2). Analytical and numerical models are being developed, to understand coupling between surface chemisorption and electronic properties. Thin-film-based gas sensors are being fabricated and studied in parallel, for comparison.
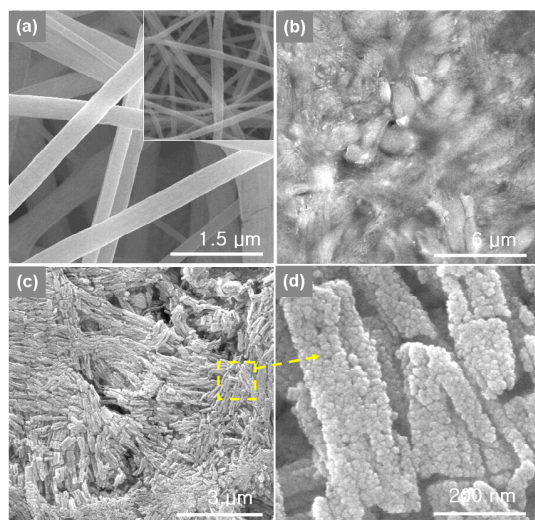
▲ Figure 1: SEM images of SnO_2 nanowires at various stages of the electrospinning process. (a) As-spun poly(vinyl acetate) / SnO_2 precursor. (b) After hot-pressing at 120°C. (c) After calcination at 450°C. (d) Magnified image, after calcination.
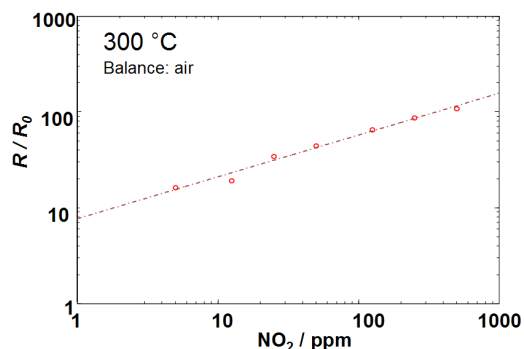
▲ Figure 2: Gas sensitivity of SnO_2 nanowire network, defined by resistance in presence of NO_2 (R) over resistance in dry air (R_0), illustrating 10-100x change in resistance for 10-1000 ppm concentration NO_2.

References

[1] F. Rock, N. Barsan, and U. Weimar, "Electronic nose: Current status and future trends," *Chemical Reviews*, vol. 108, pp. 705-725, Feb. 2008.
[2] I.D. Kim, A. Rothschild, T. Hyodo, and H.L. Tuller, "Microsphere templating as means of enhancing surface activity and gas sensitivity of $CaCu_3Ti_4O_{12}$ Thin Films," *Nano Letters*, vol. 6, no. 2, pp. 193-198, Feb. 2006.
[3] J.A. Lewis and G.M. Gratson, "Direct writing in three dimensions," *Materials Today*, vol. 7, no. 7-8, pp. 32-39, July-Aug. 2004.

# CNT-Based Open Architecture Ionizer for Portable Mass Spectrometry

L.F. Velásquez-García, A.I. Akinwande
Sponsorship: DARPA

Mass spectrometers need to ionize the sample that they are analyzing to determine its chemical composition. Traditional ionizers for gases use either chemical ionization (CI) or electron impact ionization (EII). In the latter case, electrons from thermionic sources produce ions by colliding with neutral molecules. More efficient carbon nanotube-based field-emitted electron impact ionizers have been developed [1]. However, one of the drawbacks of EII is that the sample is transformed into small fragmentation products. Several samples could have similar fragmentation spectra but be quite different compounds, with radically different properties. (For example, one substance can be a poisonous agent while another is a harmless material). Therefore, an approach to reduce the fragmentation products would improve the informational power of the mass spectrometer.

Field ionization soft-ionizes molecules, thus reducing the fragmentation products. The field ionization scheme creates ions by directly tunneling electrons from the outer shell of neutral molecules by virtue of a very high electric field [2]. The electric field is produced by high-aspect-ratio field enhancers and the application of a large (up to 1 kV) bias voltage. Carbon nanotubes (CNTs) are ideal field enhancers because of their high aspect ratio and their nanometer-sized tip radius. In the case of the EIIs, a closed architecture is implemented because it is intended to protect the field enhancers from back-streaming positive ions [3]. However, this protection is not needed in a field ionizer because in this case the field enhancers are biased at a positive voltage with respect to the gate. Also, an open architecture, where the field enhancers are accessible by the neutral molecules from all directions, is a more suitable approach to produce field ionization because it increases the ion current. We have implemented the emitting substrate of an open architecture single-gated field ionizer array [4]. The substrate is a micro-fabricated 3D foam-like silicon structure (µfoam). The µfoam is fabricated using deep reactive ion-etching (DRIE). On top of the µfoam, there is a sparse array of plasma-enhanced chemical-vapor-deposited (PECVD) CNTs (Figure 1) that act as field enhancers. The CNTs are sparsely grown to avoid field enhancer shadowing. The substrate has been tested with a triode setup. The data shows a startup ionization voltage as low as 175 V (Figure 2). Current research efforts focus on developing a gated version of the ionizer.
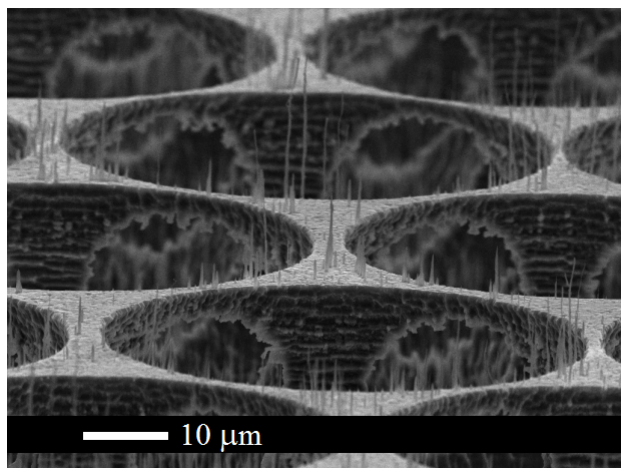
▲ Figure 1: Detail of sparse PECVD CNT cluster on the µfoam. The CNTs have 80-nm-diameter tips and are up to 14 µm tall.
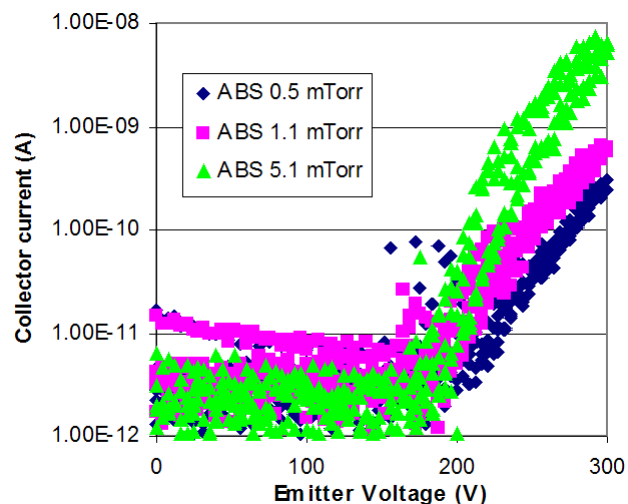
▲ Figure 2: The IV characteristics of the field ionizer. The collector is a smooth ball of 2 mm diameter hovering about 4 mm above the gate. The collector was biased at –1100 V. The gate is biased at 0 V.

References

[1] L.-Y. Chen, "Double-gated field emission arrays," Ph.D. thesis, Massachusetts Institute of Technology, Cambridge, 2007.
[2] R. Gomer, *Field Emission and Field Ionization*, New York: American Institute of Physics, 1961, rpt. 1993.
[3] L. Dvorson, I. Kymissis, and A.I. Akinwande, "Double-gated silicon field emitters," *Journal of Vacuum Science and Technology B*, vol. 21, no. 1, pp. 486-494, Jan. 2003.
[4] L.F. Velásquez-García and A.I. Akinwande, "A PECVD CNT-based open architecture field ionizer for portable mass spectrometry," *Technical Digest 21st IEEE International Conference on Microelectromechanical Systems*, Tucson AZ, Jan. 2008, pp. 742-745.

Aligned CNT-based Micro-structures and Nano-Engineered Composite Macro-structures

B.L. Wardle, R. Guzman de Villoria, N. Yamamoto, H. Cebeci, K. Ishiguro, S.A. Steiner III, S. Wicks, S. Figueredo, E.J. Garcia, A.J. Hart, H. Duong, D. Saito (in collaboration with A.H. Slocum)

Carbon nanotube (CNT) composites are promising new materials for structural applications thanks to their mechanical and multifunctional properties. We have undertaken a significant experimentally-based program to understand both micro-structures of aligned-CNT nanocomposites and nano-engineered advanced composite macro-structures hybridized with aligned CNTs.

Aligned nanocomposites were fabricated by mechanical densification and polymer wetting of aligned CNTs [1]. Unmodified high-grade epoxy resins were used as a matrix. As reinforcement, aligned-CNT forests were grown to mm-heights on a Si substrate using a modified chemical-vapor-deposition process. The forests were grown on 1-cm² Si substrates and then released from the substrate. The volume fraction of as-grown CNTs is about 1%; however, the distance between the CNTs (and thus the volume fraction of the forest) can be varied by applying a compression force in both directions of the plane of the forest, resulting in volume fractions of CNTs exceeding 20%. Nanocomposites were fabricated by infusion of the matrix into the CNT forest via capillary-induced wetting [2, 3], the rate of which depends on properties of the CNT forest (e.g., volume fraction) and the polymer (viscosity, contact angle, etc.). Variable-volume fraction-aligned CNT nanocomposites were characterized using optical, scanning electron (SEM), and transmission electron (TEM) microscopy to analyze dispersion and alignment of CNTs as well as overall morphology. Nano-engineered composite macro-structures hybridized with aligned CNTs were prepared by placing long (>20 μm) aligned CNTs at the interface of advanced composite plies as reinforcement in the through-thickness axis of the laminate. Three fabrication routes were developed: transplantation of CNT forests onto preimpregnated plies [4] (the "nano-stitch" method), placement of detached CNT forests between two fabrics followed by subsequent infusion of matrix, and *in situ* growth of aligned CNTs onto the surface of ceramic fibers followed by impregnation and hand lay-up [5]. Aligned CNTs are observed at the composite ply interfaces. Significant improvement appears in interlaminar strength and electrical properties over composites without aligned CNTs . Analysis of the multifunctional properties of and nanoscale interactions between the constituents in both the nanocomposites and hybrid macrostructures is underway.
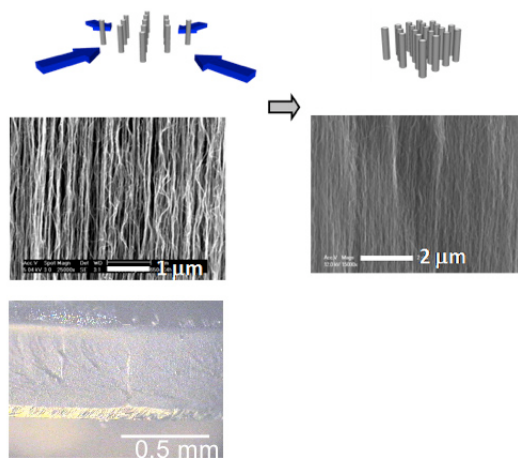
▲ Figure 1: Aligned CNT nanocomposites via biaxial mechanical densification of CNT forests.
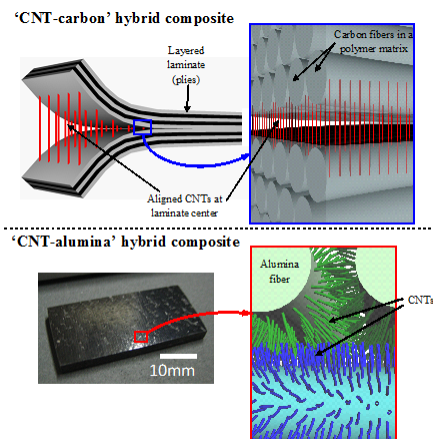
▲ Figure 2: Aligned CNT nano-engineered composite macro-scale architectures.

References

[1] B.L. Wardle, D.S. Saito, E.J. Garcia, A.J. Hart, and R. Guzman de Villoria, "Fabrication and characterization of ultra-high volume fraction aligned carbon-nanotube-polymer composites," *Advanced Materials*, vol. 20, 14, pp. 2707-2714, July 2008.

[2] E.J. García, A.J. Hart, B.L. Wardle, and A.H. Slocum, "Fabrication of composite microstructures by capillarity-driven wetting of aligned carbon nanotubes with polymers," *Nanotechnology*, vol. 18, pp. 165602:1-11, 2007.

[3] E.J. García, A.J. Hart, B.L. Wardle, and A.H. Slocum, "Fabrication and nanocompression testing of aligned carbon-nanotube-polymer nanocomposites," *Advanced Materials*, vol. 19, pp. 2151, 2007.

[4] E.J. Garcia, B.L. Wardle, and A.J. Hart, "Joining prepreg composite interfaces with aligned carbon nanotubes," *Composites Part A*, vol. 20, 14, pp. 2707-2714, June 2008.

[5] E.J. Garcia, B.L. Wardle, A.J. Hart, and N. Yamamoto, "Fabrication and multifunctional properties of a hybrid laminate with aligned carbon nanotubes grown in situ," *Composites Science and Technology*, vol. 68, 9, pp. 2034-2041, July 2008.

Catalyst Engineering and Growth Mechanisms of Si and III-V Nanowires

S.T. Boles, O.M. Nayfeh, C.K.F. Ho, D.A. Antoniadis, E.A. Fitzgerald, C.V. Thompson
Sponsorship: Singapore-MIT Alliance

The vapor-liquid-solid mechanism for growth of single crystal whiskers and wires was originally discovered in the 1960s but has only recently been rediscovered as a way to fabricate high-performance nanoscale electronic devices, with dimensions below those attainable with photolithography. Although a great deal of attention has been focused on the electronic properties of Si and III-V nanowires, many of the physical mechanisms involved in growing these single crystal wires remain unclear. We have been investigating the importance of catalyst size and shape for wire growth morphology by using evaporated island catalysts, catalysts derived from dewetted thin films, and commercially available nanoparticles. Optimizing catalyst processing conditions and combining them with specific topographies or templates, such as inverted pyramid arrays or silicon dioxide gratings, achieves precise control over catalyst placement and subsequent nanowire placement. Also in this study, the role of growth conditions has been investigated by controlling the growth temperature, the partial pressures of reactants and the conditions of pre-growth annealing. These parameters have been determined to be critical not only to stable and repeatable growth of Si and III-V nanowires, but also to controlling the relative orientation and defect generation at the substrate-wire interface.
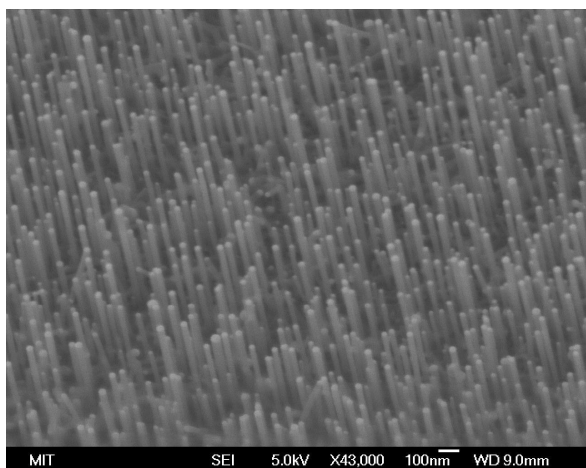
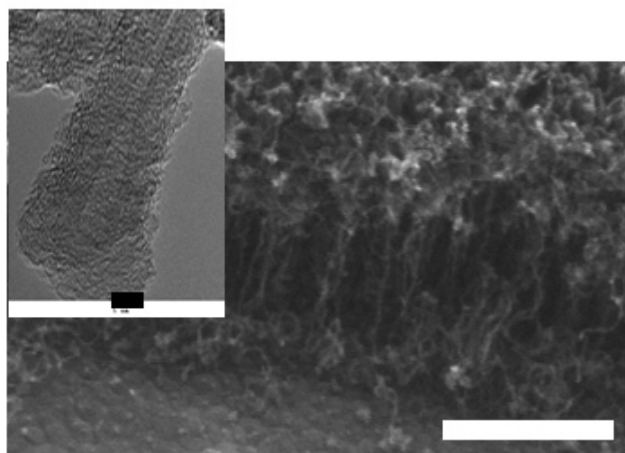▲ Figure 1: Si nanowires grown on Si <111> substrates using Au catalysts.

▲ Figure 2: GaP nanowire grown on Si <111> substrate using Ag catalyst.
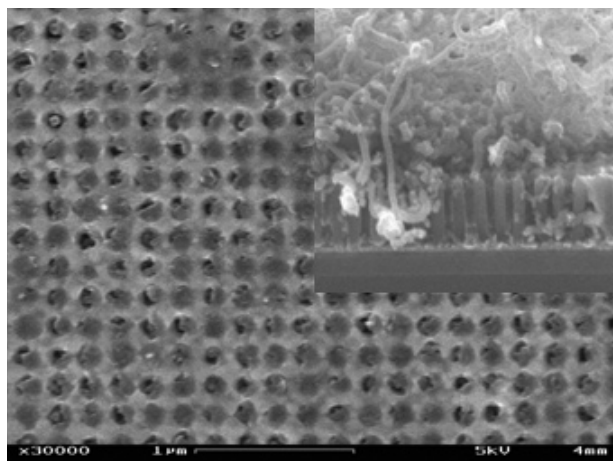
Carbon Nanotube Growth for I.C. Interconnects

G.D. Nessim, Y. Wang, A.J. Hart, D. Acquaviva, J. Oh, J.S. Kim, C. Morgan, N. Abate, M. Seita, C.V. Thompson
Sponsorship: SRC/FCRP IFC, Intel

As integrated circuit technology is developed at dimensions below 32 nm, carbon nanotubes (CNTs) represent an ideal replacement for copper interconnects as they can carry higher current densities, do not need liners, and do not suffer from electromigration. However, fabrication issues such as growing the desired type of CNTs, using CMOS-compatible processes (e.g., ideally at temperature below 400°C) and making electrical contacts and interconnections, remain major technical challenges. For electrical applications, it is important to grow CNTs on conductive substrate [1, 2]. Using appropriate catalyst/substrate metallic thin films, we have grown vertically-aligned, crystalline CNTs using thermal chemical vapor deposition at 475°C (Figure 1). Preliminary electrical measurements show ohmic contact of the CNTs with the metallic substrate.

We have also grown CNTs on conductive substrates into an insulating alumina scaffold with regularly spaced pores (Figure 2). The insulating scaffold is fabricated using interference lithography and anodization of aluminum. This structure simulates an array of nanometer-scale vias filled with CNTs. In order to have CNTs with uniform height (length) and to make electrical contact with all the walls in the multi-wall tubes, we ion-milled the tops after CNT growth. The electrical properties of these CNTs can be collectively characterized through deposition of a conducting overlayer on all the CNTs or individually characterized using an AFM on uncapped CNTs. We plan to characterize electrical properties as a function CNT diameter and length and as a function of contact metallurgy.

▲ Figure 1: Carpet of vertically-aligned CNTs on conductive substrate grown at 475°C (scale bar 500 nm). The catalyst/underlayer system is Fe/Ta. The HRTEM image on the inset shows the crystalline nature of the CNTs (scale bar 5 nm).

▲ Figure 2: The CNTs grown into alumina scaffold with pores regularly spaced. The CNTs are flush with the top surface after ion milling. The inset shows the CNTs prior to ion milling.
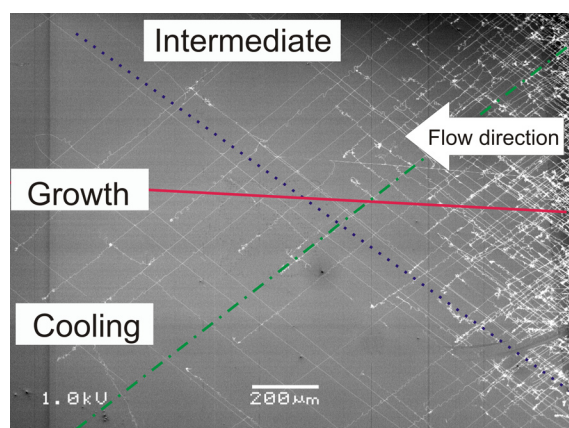
References

[1] H.T. Ng, B. Chen, J.E. Koehne, A.M. Cassell, J. Li, J. Han, and M. Meyyappan, "Growth of carbon nanotubes: A combinatorial method to study the effects of catalysts and underlayers," *Journal of Physical Chemistry B*, vol. 107, no. 33, pp. 8484-8489, 2003.

[2] S. Talapatra, S. Kar, S.K. Pal, R. Vajtai, L. Ci, P. Victor, M.M. Shaijumon, S. Kaur, O. Nalamasu, and P.M. Ajayan, "Direct growth of aligned carbon nanotubes on bulk metals," *Nature Nanotechnology*, vol. 1, no. 2, pp. 112-116, 2006.

In-situ Sample Rotation as a Tool to Understand CVD Growth of Long Aligned Carbon Nanotubes

M. Hofmann, D. Nezich, A. Reina Cecco, J. Kong

A new tool for studying the process of carbon nanotube chemical vapor deposition (CVD) synthesis is described. Rotating the substrate *in-situ* during the CVD process changes the orientation of floating nanotubes with respect to the substrate and nanotubes attached to the substrate by interaction with the gas stream (see Figure 1). Defining a time window in between consecutive rotation steps makes it is possible to study carbon nanotube behavior during CVD growth in a time-resolved manner (Figure 2). As an example, the settling process (i.e., the sinking of the nanotube to the substrate) is investigated. The analysis of forces acting on a floating nanotube shows that a vertical gas stream due to thermal buoyancy over the sample can keep long nanotubes floating for extended times. A stochastic process, indicated by a constant settling rate over time, forces the nanotube into contact with the substrate and this process is attributed to flow-induced instability. Our study reveals additional information on the floating and settling process. The authors acknowledge the support of the Interconnect Focus Center, one of five research centers funded under the Focus Center Research Program, a DARPA and Semiconductor Research Corporation program [1-4].

▲ Figure 1: An SEM picture of the aligned nanotubes after rotation with indication of corresponding experimental phases.
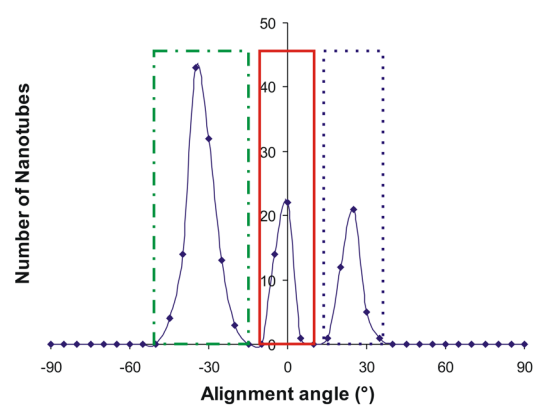
▲ Figure 2: Histogram of angular distribution of nanotubes with indication of corresponding phases.

References

[1] A. Reina, M. Hofmann, D. Zhu, and J. Kong, "Growth mechanism of long and horizontally aligned carbon nanotubes by chemical vapor deposition," *Journal of Physical Chemistry C*, vol. 111, no. 20, pp. 7292-7297, May 2007.

[2] L.X. Zheng, M.J. O'Connell, S.K. Doorn, X.Z. Liao, Y.H. Zhao, E.A. Akhadov, M.A. Hoffbauer, B.J. Roop, Q.X. Jia, R.C. Dye, D.E. Peterson, S.M. Huang, J. Liu, and Y.T. Zhu, "Ultralong single-wall carbon nanotubes," *Nature Materials*, vol. 3, no. 10, pp. 673-676, Oct. 2004.

[3] L.M. Huang, Z. Jia, and S. O'Brien, "Orientated assembly of single-walled carbon nanotubes and applications," *Journal of Materials Chemistry*, vol. 17, no. 37, pp. 3863-3874, June 2007.

[4] D. Takagi, Y. Homma, S. Suzuki, and Y. Kobayashi, "*In-situ* scanning electron microscopy of single-walled carbon nanotube growth," *Surface and Interface Analysis*, vol. 38, nos. 12-13, pp. 1743-1746, Dec. 2006.

# Growth Studies of In-plane and Out-of-plane SWNTs for Electron Devices

L.F. Velasquez-Garcia, D. Akinwande (Stanford), P. Wong (Stanford), A.I. Akinwande
Sponsorship: DARPA

Carbon nanotubes (CNTs) are currently massively investigated due to their remarkable mechanical, thermal, chemical, and electrical properties [1]. CNTs are seamless graphite tubes that can be grown using diverse methods such as arc deposition, chemical vapor deposition (CVD), and plasma-enhanced chemical-vapor-deposition (PECVD) [2]. The best performance comes from CNTs made of a single graphite sheet, i.e., single-walled carbon nanotubes (SWNTs). SWNTs are 1 – 2 nm in diameter and can have lengths over several centimeters [3]. Both in-plane and out-of-plane SWNTs are useful in the device industry. In-plane SWNTs can be used as the channel in transistors, while out-of-plane SWNTs can be used in circuit vias. We are currently investigating the growth of CVD SWNTs using our PECVD reactor. A forest of in-plane SWNTs can be grown using a methane/hydrogen chemistry at 200 Torr and 880°C if 2 Å Fe is used as a catalyst on top of quartz substrates (Figure 1). Sparse forests can be formed at lower pressures and temperatures (Figure 2). Current research focuses on investigating the growth space for in-plane SWNTs and developing growth recipes for out-of-plane SWNTs. With this information, devices will be designed and implemented.
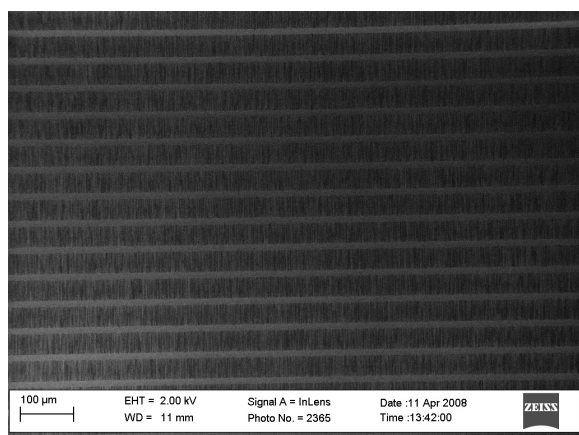
▲ Figure 1: A forest of in-plane SWNTs grown at 880°C and 200 Torr if iron is used as catalyst with a hydrogen/methane mix. The substrate is quartz.
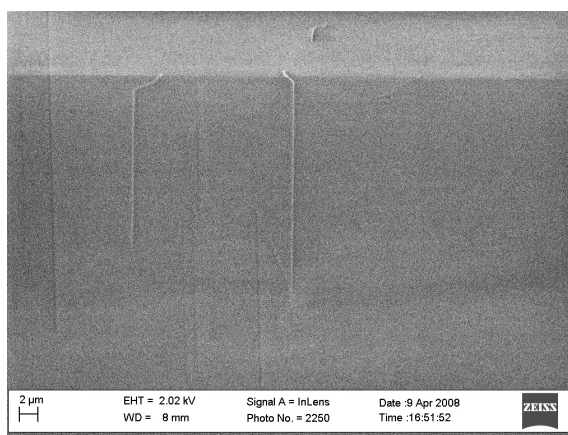
▲ Figure 2: Sparse growth of in-plane SWNTs occurs if iron is used as a catalyst in a hydrogen/methane mix at 825°C and 100 Torr. The substrate is quartz.

References

[1] S. Iijima, "Helical microtubules of graphitic carbon," *Nature*, vol. 354, no. 6348, pp. 56-58, 1991.

[2] K.B.K. Teo, S.-B. Lee, M. Chhowalla et al., "Plasma-enhanced chemical vapour deposition carbon nanotubes/nanofibers –How uniform do they grow?" *Nanotechnology*, vol 14, pp. 204-211, 2003.

[3] H.W. Zhu, C.L. Xu, D.H. Wu, B.Q. Wei, R. Vajtai, and P.M. Ajayan, "Direct synthesis of long single-walled carbon nanotube strands," *Science*, vol. 296, no. 5569, pp. 884-886, 2002.

High-current CNT FEAs on Si Pillars

L.F. Velásquez-García, Y. Niu, A.I. Akinwande
Sponsorship: DARPA, AFOSR

Electrons are field-emitted from the surface of metals and semiconductors when the potential barrier (work function) that holds electrons within the metal or semiconductor is deformed by the application of a high electrostatic field. Field emitters use high-aspect-ratio structures with tips that have nanometer dimensions to produce a high electrostatic field with a low applied voltage. Small changes in the tip radius result in huge changes in the current density because of the exponential dependence of the emitted current on the bias voltage, as described by the Fowler-Nordheim theory. Also, tip radii variation in an array results in non-uniform turn-on voltages. If the emitters are ballasted, the spatial non-uniformity can then be substantially decreased. Furthermore, ballasting individual emitters prevents destructive emission from the sharper tips, resulting in higher overall current emission because of the inclusion of duller tips. Ballasting also results in more reliable operation. The use of large resistors in series with the field emitters is an unattractive bal-

lasting approach because of the resulting low emission currents and power dissipation in the resistors. A better approach for ballasting field emitters is the use of ungated field-effect transistors (FETs) that effectively provide high dynamic resistance with large saturation currents [1]. In the past our research group demonstrated the use of a MOSFET to ballast the emission of electrons from silicon tips [2]. We have implemented a large and dense array of plasma-enhanced chemical-vapor-deposited (PECVD) carbon nanotubes (CNTs) (1-million elements in 1 cm2), in which each emitter is individually ballasted by a high-aspect-ratio column that acts as an ungated FET (Figure 1) [3]. For an n-Si substrate with a high-enough doping level, the Fowler- Nordheim (FN) plot of the data shows no saturation (Figure 2). Current research focuses in systematically studying the dependence of the ballasting on the doping level, showing current limiting data using CNT FEAs, and implementing a gated version of the field-emitter array.
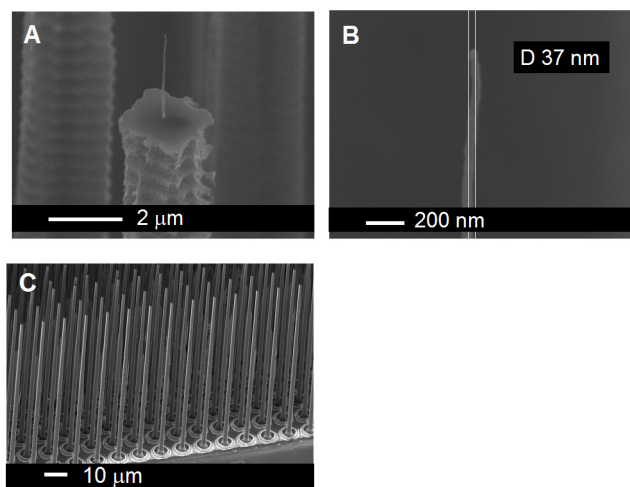
▲ Figure 1: A PECVD CNT on top of a high-aspect-ratio Si column that acts as an ungated FET to limit the emitter current (A). The CNT is about 4 μm tall and it has 37-nm diameter (B). The FETs are 100 μm tall and have less than 1 μm × 1 μm cross-section (C).
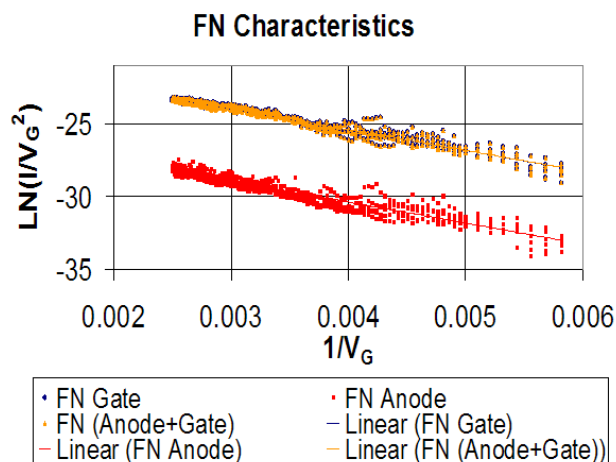
▲ Figure 2: Fowler–Nordheim plot for a 10^6 CNT emitter array that uses an n-Si substrate with doping level equal to 1×10^{15} cm^{-3}. The FN model describes the electron current of the device because the doping level of its FETs is not low enough to produce current limitation.
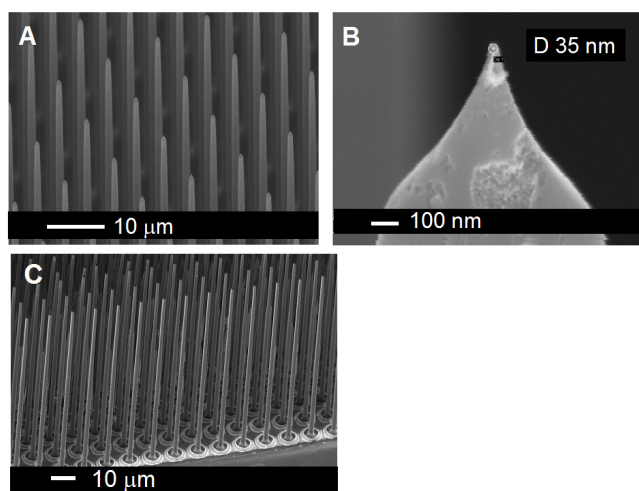
References

[1] C.-Y. Hong and A.I. Akinwande, "Temporal and spatial current stability of field emission arrays," *IEEE Transactions on Electron Devices*, vol. 52, no. 10, pp. 2323–2328, Oct. 2005.

[2] H. Takemura, et. al., "A novel vertical current limiter fabricated with a deep-trench-forming technology for highly reliable field emitter arrays," *Technical Digest of the IEEE International Electron Device Meeting*, Dec. 1997, pp. 709–712.

[3] L.F. Velásquez-García, B. Andeoti, Y. Niu, and A.I. Akinwande, "Uniform high-current field-emission of electrons from Si and CNF FEAs individually controlled by Si pillar ungated FETs," *Technical Digest IEEE International Electron Device Meeting*, Washington DC, Dec. 2007, pp. 599–602.

High-current Si FEAs on Si Pillars

L.F. Velásquez-García, Y. Niu, A.I. Akinwande
Sponsorship: DARPA, AFOSR

Electrons are field-emitted from the surface of metals and semiconductors when the potential barrier (work function) that holds electrons within the metal or semiconductor is deformed by the application of a high electrostatic field. Field emitters use high- aspect-ratio structures with tips that have nanometer dimensions to produce a high electrostatic field with a low applied voltage. Small changes in the tip radius result in huge changes in the current density because of the exponential dependence of the emitted current on the bias voltage, as described by the Fowler-Nordheim theory. Also, tip radii variation in an array results in non-uniform turn-on voltages. If the emitters are ballasted, the spatial non-uniformity can then be substantially decreased. Furthermore, ballasting individual emitters prevents destructive emission from the sharper tips, resulting in higher overall current emission because of the inclusion of duller tips. Ballasting also results in more reliable operation. The use of large resistors in series with the field emitters is an unattractive ballasting approach because of the resulting low emission currents and power dissipation in the resistors. A better approach for ballasting field emitters is the use of ungated field-effect transistors (FETs) that effectively provide high dynamic resistance with large saturation currents [1]. In the past our research group demonstrated the use of a MOSFET to ballast the emission of electrons from silicon tips [2]. We have implemented a large and dense array of conical Si tips (1 million elements in 1 cm²), where each emitter is individually ballasted by a high-aspect-ratio column that acts as an ungated FET (Figure 1) [3]. The Fowler- Nordheim (FN) plot of the data for lowly doped arrays shows that the ungated FETs limit the emitter current because the slope of the curve becomes horizontal for high-enough current levels (Figure 2). We have obtained electron currents as large as 10 mA, the largest field-emitted currents reported from Si tips. Current research focuses on systematically studying the dependence of the ballasting on the doping level and implementing a gated version of the array.

▲ Figure 1: An array of silicon field emitters individually ballasted by vertical ungated FETs (A). The field emitter diameter is about 35 nm (B). The FETs are 100 µm tall and have a less than 1 µm × 1 µm cross-section (C).
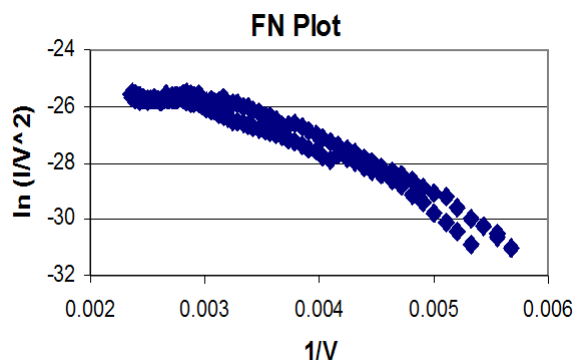
▲ Figure 2: Fowler-Nordheim plot for a 4000 Si emitter array that uses an n-Si substrate with doping level equal to 2×10^{13} cm^{-3} For unballasted field emitters, the curve is a straight line. The current is limited to the point that the curve becomes horizontal for high enough voltages.

References

[1] C.-Y. Hong and A.I. Akinwande, "Temporal and spatial current stability of field emission arrays," *IEEE Transactions on Electron Devices*, vol. 52, no. 10, pp. 2323-2328, Oct. 2005.

[2] H. Takemura, et. al., "A novel vertical current limiter fabricated with a deep-trench-forming technology for highly reliable field emitter arrays," *Technical Digest of the IEEE International Electron Device Meeting*, Dec. 1997, pp. 709-712.

[3] L.F. Velásquez-García, B. Andeoti, Y. Niu and A.I. Akinwande, "Uniform high-current field-emission of electrons from Si and CNF FEAs individually controlled by Si pillar ungated FETs," *Technical Digest IEEE International Electron Device Meeting*, Dec. 2007, pp. 599- 602.

Compound Semiconductor Nanowire Heterostructures for High-mobility Electronics

M.J. Tambe, S. Gradečak
Sponsorship: 3M Inc., SRC/FCRP IFC 674.017

Semiconductor nanowires have emerged as a promising new platform for nanoscale electronics. With improved interfacial properties, more efficient strain relaxation, and reduced dimensionality, nanowire heterostructures have been predicted to be synthesizable with carrier mobilities significantly greater than bulk values. Since the carrier mobility of GaAs-based materials is intrinsically high, GaAs/AlGaAs nanowire heterostructures are an ideal candidate for nanowire high-mobility transistor applications. We propose to synthesize core-shell GaAs/AlGaAs nanowire heterostrucutres to study the potential benefits of nanostructuring on electronic transport properties as well as develop techniques to fabricate modulation-doped high-mobility nanowire transistors.

Radially-modulated core-shell GaAs/AlGaAs nanowire heterostructures have been synthesized by metal-organic chemical vapor deposition (MOCVD). Scanning electron microscopy (SEM) images show these wires grow vertically aligned with over 80% of the deposited catalyst nanoparticles yielding core-shell nanowires (Figure 1a, Figure 1b). Chemical analysis by energy dispersive X-Ray spectroscopy (EDS) reveals the composition of the core and shell to be GaAs and $Al_{0.9}Ga_{0.1}As$, respectively (Figure 1c). Structural analysis of the nanowires by transmission electron microscopy (TEM) confirms epitaxial shell deposition free of structural defects such as dislocations, stacking faults, and twin planes (Figure 1d, Figure 1e). The electronic transport properties of nanowires are studied by forming basic transistor structures. The nanowires are deposited onto degenerately doped Si/SiO_2 wafers and then Ohmic NiGeAu contacts are defined by e-beam lithography and deposited by e-beam evaporation. The top contacts serve as source and drain contacts while the gate contact is placed on the backside of the wafer using the top oxide as the gate oxide (Figure 2).
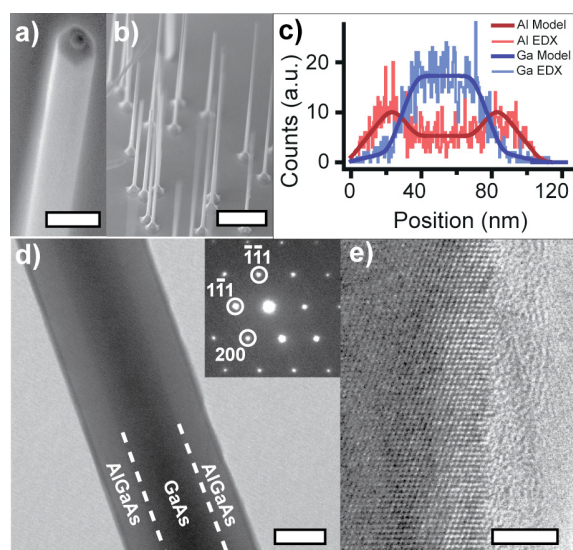
▲ Figure 1: a) SEM image of core-shell nanowire tip. b) SEM image of vertically aligned nanowires. c) EDX linescan analysis of a core-shell nanowire in planview. d) Bright-field TEM image of a core-shell nanowire showing clear core-shell contrast. (inset is SAD pattern along 011 zone axis) e) High-resolution TEM image of defect-free epitaxial AlGaAs shell.
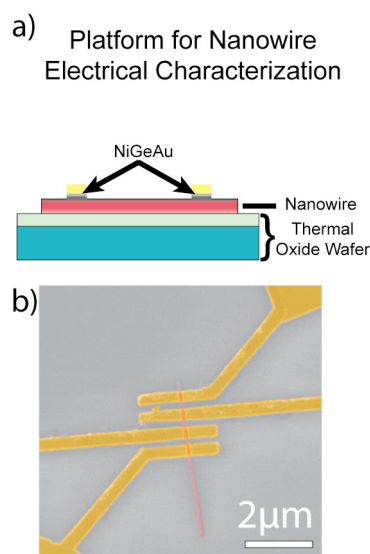
▲ Figure 2: a) Schematic of a nanowire transistor for materials electrical characterization. b) False-colored SEM image of fabricated nanowire device.

Anodic Aluminum Oxide Scaffolds and Metallic Nanowires for Sensor Applications

J. Oh, S. Cui, C.V. Thompson
Sponsorship: FCRP, Singapore-MIT Alliance

Metallic nanowires are core building blocks for advanced functional devices such as chemical and biochemical sensors [1]. To integrate nanowires into devices, it is desirable to fabricate them with controlled sizes and locations on device-applicable substrates. As a strategy for this goal, we are developing templated self-assembly methods that combine top-down (lithography) and bottom-up (self-assembly) approaches for fabrication and assembly of metallic nanowires for chemical and biochemical sensor applications, including a glucose biosensor [2].

Ordered porous alumina (OPA) is a nano-structured material that self-orders with domains and has been widely used as a template for growth of metallic nanowires, using electrochemical deposition techniques. However, growth of nanowires in OPA to make electrical contact to conducting underlayers is blocked by thin insulating barrier-oxide layers at the base of the pores, and removing these barriers without pore-widening due to etching [3-4] is desirable.

A new method for perforation of the OPA barrier layer has been developed based on anodization of Al/W multilayer films on substrates. When Al/W multilayer films are anodized and pores approach the Al/W interface, tungsten oxide forms and penetrates the alumina barrier oxide. By selectively etching the tungsten oxide, the barrier oxide can be removed and the base of the pores opened, without etching of the OPA (Figure 1). With this technique, we demonstrated that it is possible to perforate OPA barrier layers for porous structures with small-diameter pores at small spacings and fabricated free-standing metallic nanowires of materials such as Ni, Au, and Pt on Si substrates (Figure 2) by selectively removing the OPA template [5]. By modifying the surface of those nanowires, we are building a biosensor to detect glucose for diagnostics of diabetes.
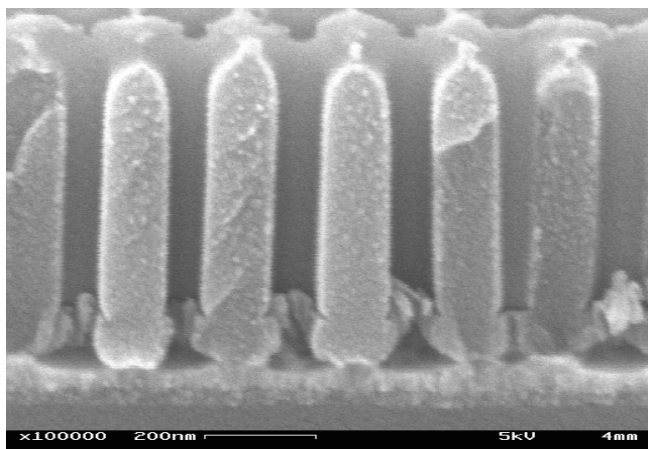
▲ Figure 1: Cross-sectional SEM image of OPA after removal of thin barrier oxide.
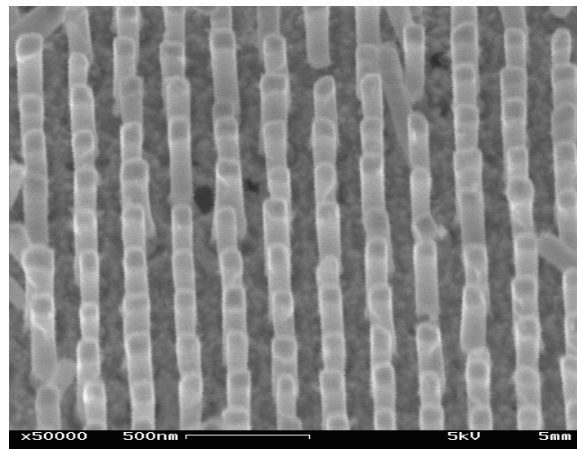
▲ Figure 2: An SEM image of free-standing Ni nanowires on conducting layer on Si substrates.

References

[1] F. Favier, E.C. Walter, M.P. Zach, T. Benter, and R.M. Penner, "Hydrogen sensors and switches from electrodeposited Pd mesowire arrays," *Science*, vol. 93, pp. 2227-2231, Sept. 2001.

[2] R. Krishnan and C.V. Thompson, "Monodomain high-aspect-ratio 2D and 3D ordered porous alumina structures with independently controlled pore spacing and diameter," *Advanced Materials*, vol. 19, pp. 988-992, Apr. 2007.

[3] O. Rabin, P.R. Herz, Y.-M. Lin, A.I. Akinwande, S.B. Cronin, and M.S. Dresselhaus, "Formation of thick porous anodic alumina films and nanowire arrays on silicon wafers and glass," *Advanced Functional Materials*, vol. 13, pp. 631-638, Aug. 2003.

[4] K. Nielsch, F. Müller, A.P. Li, and U. Gösele, "Uniform nickel deposition into ordered alumina pores by pulsed electrodeposition," *Advanced Materials*, vol. 12, pp. 582-586, Apr. 2000.

[5] J. Oh and C.V. Thompson, "Selective barrier perforation in porous alumina anodized on substrates," *Advanced Materials*, vol. 20, pp. 1368-1372, Apr. 2008.
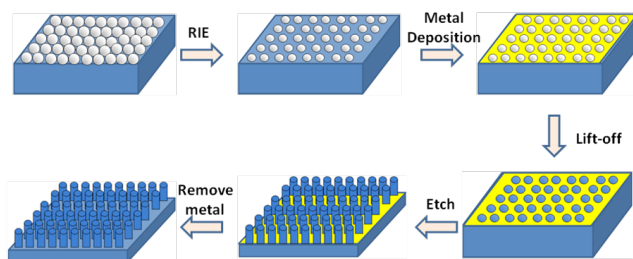
Silicon Nanowire Fabrication by Metal-assisted Etching

S.-W. Chang, C.V. Thompson
Sponsorship: Singapore-MIT Alliance

Pore formation under anodic conditions is a well-known phenomenon for many semiconductors. However, the anodization approach to etching requires conductive substrates and independent control of a relatively large number of process parameters. To circumvent these problems, an electrochemical etching method known as metal-assisted etching (MAE) has recently received significant attention. In this approach metal catalysts are used to enhance local Si etching at the metal-silicon interface, in a mixture of hydrofluoric acid and an oxidant. The process can be used to fabricate high-aspect-ratio Si structures through patterned etching of silicon wafers. For example, we and others have used this technique to develop a relatively simple method for producing ordered arrays of one-dimensional silicon nanostructures over large areas via the combination of nanosphere lithography (NSL) and MAE.

In this approach, NSL is used to fabricate an ordered array of nanoscopic holes perforated in metal thin films. The process begins with the formation of a two-dimensional, self-assembled monolayer of monodisperse nanospheres. Typical domain sizes are in the 10-100-μm range [1]. A dry etching step is carried out to reduce the diameter of the nanospheres. A metal thin film is subsequently deposited through the nanosphere mask using electron beam (e-beam) evaporation. After metal deposition, the nanospheres can be selectively removed to leave behind only the metal deposited through the mask. Using this nanoporous film as a catalyst for silicon etching produces an ordered array of silicon nanopillars with the same diameter as the original pores. Figure 1 shows a schematic of the process flow. Figure 2 shows SEM images of a silicon nano-pillar array after etching. As can be seen in the lower magnification image on the left, the wires are very uniform in length, suggesting a uniform etch rate over large areas.

▲ Figure 1: Process flow for the fabrication of unpatterned 1D Si nano-pillars.
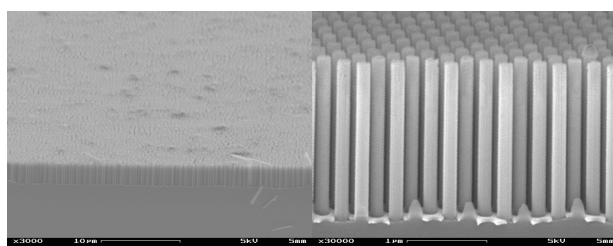
▲ Figure 2: Silicon nano-pillars fabricated using NSL and metal-assisted etching.

Reference
[1]   G. Schmid, *Clusters and Colloids from Theory to Applications.*. New York, NY: Wiley-VCH, 1994.

# Nano-particle Formation via Solid-state Dewetting

A.L. Giermann, J. Ye, Y. Wang, D. Kim, H. Yu, T.H. Liew, J. Yun, W.K. Choi, C.V. Thompson
Sponsorship: Singapore-MIT Alliance, NSF

We are investigating solid-state dewetting of thin films as a technique for producing ordered arrays of metal nanoparticles over large areas. Such arrays are used as catalysts for nanowire and nanotube growth and may also be of interest in memory or plasmon device applications.

When we begin with a single crystalline film, the dewetted nano-islands align along specific crystallographic orientations and show regular patterns. We observe a strong dependence of the morphological evolution of single crystalline nickel thin films on the thickness of the film and on the crystallographic orientation of the film, which is determined by an epitaxial relationship with a magnesium oxide substrate. The resulting nanoparticles remain epitaxial and thus share both in- and out-of -plane crystallographic alignment.

In order to obtain similarly ordered dewetting with polycrystalline films, we employ physical templates. One technique is to physically constrain the area of film that dewets by pre-patterning a polycrystalline gold film on silicon dioxide. We observe that certain geometries lead to self-alignment of the dewetted nanoparticles (see Figure 1). Ongoing investigations will further characterize how film thickness and pattern dimensions affect the self-alignment.

Another technique for ordered dewetting of polycrystalline films is the use of topographic templates to modulate the curvature of as-deposited films. Gold films dewetted on di-periodic arrays of oxidized pyramidal pits in silicon result in one-to-one self-assembly of ordered arrays of gold particles over large areas. Compared to dewetting on flat substrates, the templates impose a significant decrease in average particle size and ensure a narrow size and spatial distribution. In this case, this technique results in crystallographic ordering of the particles, imposing an in-plane texture and changing the out-of-plane texture [1]. We observe similar spatial ordering behavior with other materials, including nickel (see Figures 2a and 2b) and cobalt; however, these materials have not demonstrated the crystallographic ordering effect. We have also combined pre-patterning with dewetting on topography to produce monodisperse Au particles. Heating allows controlled evaporation to produce populations of particles with smaller average size and a narrowed distribution of sizes (see Figures 2c and 2d) [2].

(a)

(b)
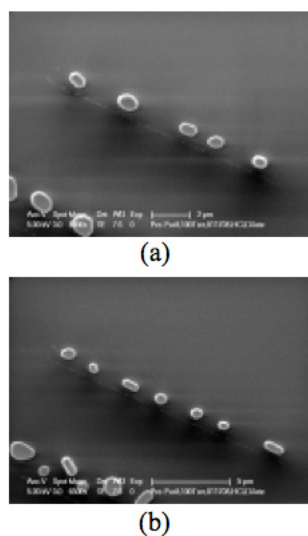
▲ Figure 1: Rows of Au particles formed by dewetting of 30-nm-thick films as a) 1.3 μm x14.5 μm and b) 1.3 μm x18 μm.

(a)

(b)

(c)

(d)
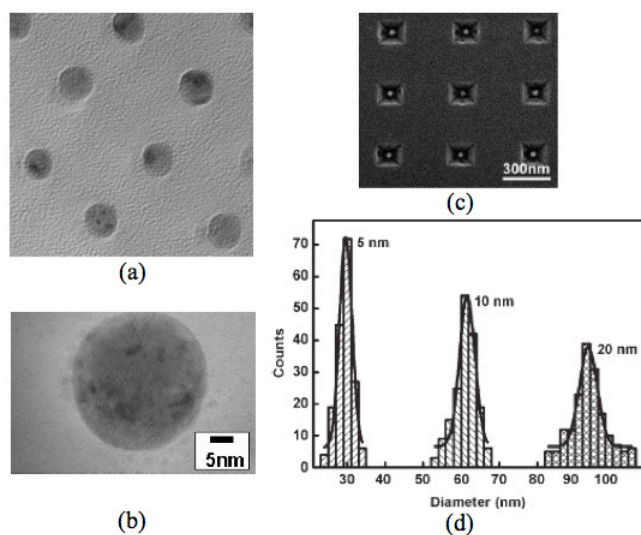
▲ Figure 2: Solid-state dewetting on substrates with inverted pyramid array topographies. (a and b) Transmission electron micrographs of ordered Ni nanoparticles. (c) Scanning electron micrograph of Au nanoparticles. (d) Distribution of nanoparticle diameters obtained by annealing Au layers with thicknesses of 5 nm, 10 nm and 20 nm at 1000 °C for 60 min.

References

[1] A.L. Giermann and C.V. Thompson, "Solid-state dewetting for ordered arrays of crystallographically oriented metal particles," *Applied Physics Letters*, vol. 86, p. 121903, Mar. 2005.
[2] W.K. Choi, T.H. Liew, H.G. Chew, F. Zheng, C.V. Thompson. Y. Wang, M.H. Hong, X.D. Wang , L. Li, and J. Yun, "A combined top-down and bottom-up approach for precision placement of metal nanoparticles on silicon," *Small*, vol. 4, no. 3, p. 330, 2008.